ISTANBUL TECHNICAL UNIVERSITY ★ GRADUATE SCHOOL OF SCIENCE
ENGINEERING AND TECHNOLOGY

DESIGN AND DEVELOPMENT OF AN FPGA CONTROLLED SILICON PIN PHOTODIODE DETECTOR ARRAY FOR NEUTRON DETECTION

Ph.D. THESIS

Ahmet BAYRAK

Department of Physics Engineering

Physics Engineering Programme

MAY 2019

ISTANBUL TECHNICAL UNIVERSITY ★ GRADUATE SCHOOL OF SCIENCE ENGINEERING AND TECHNOLOGY

DESIGN AND DEVELOPMENT OF AN FPGA CONTROLLED SILICON PIN PHOTODIODE DETECTOR ARRAY FOR NEUTRON DETECTION

Ph.D. THESIS

Ahmet BAYRAK
(509122101)

Department of Physics Engineering

Physics Engineering Programme

Thesis Advisor: Prof. Dr. Cenap Ş. ÖZBEN

MAY 2019

İSTANBUL TEKNİK ÜNİVERSİTESİ ★ FEN BİLİMLERİ ENSTİTÜSÜ

NÖTRON DETEKSİYONU İÇİN FPGA KONTROLLÜ SİLİKON PIN FOTODİYOT DETEKTÖR DİZİSİ TASARIM VE GELİŞTİRİLMESİ

DOKTORA TEZİ

Ahmet BAYRAK
(509122101)

Fizik Mühendisliği Anabilim Dalı

Fizik Mühendisliği Programı

Tez Danışmanı: Prof. Dr. Cenap Ş. ÖZBEN

MAYIS 2019

Ahmet BAYRAK, a Ph.D. student of ITU Graduate School of Science Engineering and Technology 509122101 successfully defended the thesis entitled "DESIGN AND DEVELOPMENT OF AN FPGA CONTROLLED SILICON PIN PHOTODIODE DETECTOR ARRAY FOR NEUTRON DETECTION", which he prepared after fulfilling the requirements specified in the associated legislations, before the jury whose signatures are below.

Thesis Advisor :	**Prof. Dr. Cenap Ş. ÖZBEN** Istanbul Technical University	....
Jury Members :	**Prof. Dr. Suat ÖZKORUCUKLU** Istanbul University	....
	Prof. Dr. Uğur YAHŞİ Marmara University	....

Date of Submission : **6 May 2019**
Date of Defense : **20 May 2019**

" to my family "

FOREWORD

First of all, I would like to thank to Prof. Dr. Cenap Ş. Özben, whom I believe that we have accomplished great work for many years, for his limitless support, guidance and assistance since my undergraduate years not only for academical manner but also sharing his life experiences.

Prof. Dr. Suat Özkorucuklu, Assoc. Prof. Dr. Baki Altuncevahir and Assoc. Prof. Dr. Ali Gelir have made valuable contributions to this thesis work and I thank them for their constructive cristisms to make this thesis better.

The Scientific and Technological Research Council of Turkey (TÜBİTAK) have made important contribution to this thesis work by supporting me to conduct research at Brookhaven National Laboratory (BNL), Upton-NY. I would like to thank to Dr. Sergio Rescia from BNL Instrumentation Division and Prof. Dr. Yannis K. Semertzidis from BNL Physics Department for their supports and guidances. TÜBİTAK aslo supported me through 2214-A program for conducting research at Deutsches Elektronen-Synchrotron (DESY), Hamburg-Germany. I appreciate Assoc. Prof. Dr. Altan Çakır, Dr. Ingrid-Maria Gregor and Dr. Marcel Stanitzki who gave me an opportunity to be at DESY and allowing me to take advantage of working at DESY.

Thank you very much to Edoardo Rossi and Jan Dreyling-Eschweiler for their kind helps and making me spent pleasant time at DESY.

I would like to thank my colleagues Dr. Esra Barlas Yücel, Dr. Mete Yücel and Dr. M. Erhan Emirhan for their friendships and contribution to my thesis.

Finally, I would like to thank to my precious family for their limitless support throughout my education. It is great you have been always with me and I am proud of to be your son.

May 2019 Ahmet BAYRAK
(Physics Eng.)

TABLE OF CONTENTS

Page

ABBREVIATIONS

Si	: Silicon
PIN	: P-Intrinsic-N
PE	: Polyethylene
HDPE	: High Density Polyethylene
Am-Be	: Americium Beryllium
Ci	: Curie
D-D	: Deuterium Deuterium
D-T	: Deuterium Tritium
CSP	: Charge Sensitive Preamplifier
JFET	: Junction Field Effect Transistor
mV	: Milli Volt
kV	: Kilo Volt
FPGA	: Field Programmable Gate Array
GUI	: Graphical User Interface
ns	: Nano Second
Raspi	: Raspberry PI
GPIO	: General Port for Input and Output
UART	: Universal Asynchronous Receiver-Transmitter
Tx	: Tranmission
Rx	: Receive
TRx	: Transmitter-Receiver
kbit	: Kilobit
ASCII	: American Standard Code for Information Interchange
MCA	: Multi Channel Analyzer
NIM	: Nuclear Instrumentation Module
USB	: Universal Serial Bus
DC	: Direct Current
RAM	: Random Access Memory
HDL	: Hardware Description Language
VHDL	: VHSIC Hardware Description Language
VHSIC	: Very High Speed Integrated Circuit
ASIC	: Application Specific Integrated Circuit

LIST OF TABLES

LIST OF FIGURES

Page

DESIGN AND DEVELOPMENT OF AN FPGA CONTROLLED SILICON PIN PHOTODIODE DETECTOR ARRAY FOR NEUTRON DETECTION

SUMMARY

Silicon PIN photodiodes have been widely used for detecting ionizing radiation, especially in the last decade. They can be used in wide range of applications, from the measurements of environmental radiation to X-ray imaging. These detectors can also be used for instance at accelerator facilities for beam loss monitoring and in accelerator tunnels for safety purposes.

Silicon PIN photodiodes can be used for the detection of neutrons when a special converter material is used. ^{10}B and ^{6}LiF are widely used materials for converting thermal neutrons to charged particles. These nuclei emit alpha particles and Tritons respectively followed by the absorption of thermal neutrons. Alpha particles and Tritons can be easily detected using a Silicon PIN photodiode since they have charge. In case of fast neutrons, polyethylene $(C_2H_4)_n$ is one of the most frequently used converter material because of its high hydrogen content and its availability. Fast neutrons knock out the protons from hydrogen and they can reach Silicon detector positioned next to the converter material and deposit some energy in it. When these free protons reach the detector, they can deposit some energy in Silicon latis and produce an electrical signal.

Studies showed that the production and the absorption rate of the secondary particles becomes more or less constant above a certain converter thickness (usually few hundreds of microns). For that reason, the converter materials to be tested were chosen to be thicker than 1 mm.

Most detector designs using Silicon PIN photodiodes are limited to the use of a single sensor with relatively small active surface area. The electronics and control units of these designs are mostly made from commercially available and expensive equipment. In this thesis work, an alternative to the available neutron detectors has been developed with complete electronics and control units. The detector has been developed using low-cost, windowless 9 Silicon PIN photodiodes from First Sensor company with model number PS100-CER-PIN2 and its surface is covered with a variety of hydrogen-rich converter materials.

There is an independent signal readout electronics for each individual sensor element for the designed neutron detector. These consist of JFET based charge sensitive preamplifiers and OP-AMP based shaping amplifiers. The preamplifier is the first stage of the amplification and its noise figures are very important for the detection of low energy protons. The signals from each sensor channel are processed independently. The amplitude of signals exceeding a certain threshold are digitized by means of a single bit analog digital converter circuit element for each channel independently. Finally, the digital signals are counted separately for the time duration determined by the user by means of an FPGA processor. Counting of digital signals is carried out by a system designed in FPGA processor which is operated with 100 MHz clock signal.

The *Multi Channel Counting System* consists of five sub-units. The most important of these is the *Pulse Counter Module* that reads each sensor (photodiode) channel independently and performs the counting process. This main unit, which has nine different counter units underneath, acts as a kind of interface and performs the task of receiving and distributing control information to the sub-units from a single source. Furthermore, the process of collecting data from individual pulse counters and transferring them to another relevant unit when the counting process is completed is also managed here.

An edge detector has been located at the entrance of each counter unit. Such detector samples the signal line for each clock cycle and compares the value to that of the previous reading. This eliminates the false signals. In doing so, it takes advantage of the fact that the actual signals are of different voltage values over the next two clock cycles. As soon as the edge detector detects this difference, it detects an edge and determines the actual signal. Faulty signals (for instance large noise spikes) are often of very short duration or, in other words, high frequency. In the tests performed with the signal generator, it was clearly observed that the count value obtained was consistent with the frequency value of a signal similar to the detector output supplied to the system. The counters are designed with a 24-bit ($16x10^6$) counting capacity. 24-bit resolution was found to be sufficient for the tests performed.

The entire system performs counting operations under the control of another module, the timer unit or *Stop Watch Module*, that controls the measurement time. The counting process continues for the specified time in this module and it is terminated with a signal coming out when the time expires. Then, the counting data obtained from each counter sub-unit is sent to the data editing module. It will be held there until it is transferred to the next module, Raspberry Pi.

The *Data Organizer Module* is a RAM block defined within the FPGA processor. This module manages the process of sending 24-bit count data from independent counters to the analysis medium, respectively. In this application, a standard communication protocol serial link is used. Since the maximum data size that can be transmitted on this line is limited to 8-bits, nine 24-bit count data must be divided into 8-bit parts and sent to Raspberry Pi. Then, the data is transferred to the *UART Module* which manages the communication process in 8-bit segments and finally the transmission is performed.

The *UART Module*, which manages the communication between Raspberry Pi and FPGA, is designed to operate at a speed of 115200 bits/s. This speed is also the maximum transmission speed achievable with the UART line, independent of FPGA. The *UART Module* not only allows data to be transmitted to the Raspberry Pi but also it passes the receiving command information from the Raspberry Pi to the FPGA. The received information is then transferred to the *Device Control Module*, the relevant commands are processed and executed.

Three types of commands are defined in the current version of the system. Each command is mapped to an ascii character, to be able to provide an 8-bit communication method. Accordingly, the "*01000001*" byte corresponding to the "*A*" character is the defined command related to the start of the measurement, the "*01000010*" byte corresponding to the "*B*" character stops the measurement and the "*01000011*" byte corresponding to the "*C*" character is the defined command for the system reset.

The process of sending above mentioned commands to FPGA or converting measurement data from FPGA into meaningful information is carried out entirely in Raspberry Pi. This process is managed by a program with a graphical user interface in Python. Accordingly, by pressing certain buttons, the relevant commands can be easily sent to the FPGA and the operation of the system can be controlled with a GUI.

On the Raspberry Pi side, during the acquisition and editing of the measurement results from the FPGA, the program stays in listening mode on the communication link. In the data exchange process, the two sides of the communication link are relatively synchronized with a particular byte defined. Accordingly, the program checks whether the first byte received is the starting byte defined in the program. This header byte, defined as 127 in decimal and "*01111111*" in binary, is the precursor to the next 27 byte count data. After having this first byte, the program performs a total of 9 block data retrieval processes by taking the following bytes in triple blocks. Although there is a possible 28^{th} byte for any reason, this process is limited to 27 bytes. A new data acceptance is only possible with the return of the original header byte.

After the data acquisition process is completed, the count values obtained from each sensor channel are shown on the graphical user interface screen, indicating the name of the respective channel. Each data shown here is simultaneously recorded to individual text files for each channel.

The FPGA-based measurement system successfully performs the task of creating a compact device. However, in order to obtain more detailed tests of the detector, some spectroscopic measurements are performed to obtain the energy spectra. For this purpose, instead of the existing shaping amplifiers, signal from the output of a charge sensitive preamplifier for a single channel was connected to the Canberra Model 2020 NIM spectroscopy amplifier. The amplification gain and the shaping time constant are easily adjustable with model 2020.

The first spectroscopic measurements was based on the detection of alpha rays emitted by ^{226}Ra source. Since the height of the signal to be generated by the protons formed in the Silicon material was unknown, the measurements with the alpha source of known energy were thought to be useful for correctly adjusting the gain of the amplifier. Therefore, alpha spectrum of ^{226}Ra source was taken.

Different hydrogen-rich materials were used as the converter material in the neutron measurements after the alpha source tests. High density polyethylene (HDPE), paraffin, plexiglass, FR4 and Silicon were used in the measurements performed simultaneously with the FPGA counting and the commercial spectroscopic system. It was seen that the measurement results of both systems yielded concordant results above a certain threshold.

From the Am-Be neutron source ^{241}Am, it was possible to observe the 59 keV gamma ray emitted as well as the alpha particle. It was determined that an amplification gain of 10, higher than that used in neutron measurements ,should be used in the measurements using ^{241}Am, ^{152}Eu, ^{207}Bi, ^{137}Cs and ^{60}Co sources. Due to the low signal amplitudes of gamma rays, it was observed that there was no significant contribution to the neutron based counts.

NÖTRON DETEKSİYONU İÇİN FPGA KONTROLLÜ SİLİKON PIN FOTODİYOT DETEKTÖR DİZİSİ TASARIM VE GELİŞTİRİLMESİ

ÖZET

Silicon PIN fotodiyotlar uzun yıllardır iyonize radyasyonun deteksiyonu için kullanılmaktadır ve özellikle son yıllarda çevresel radyasyon ölçümlerinden, X-ışını görüntülemeye kadar pek çok farklı uygulamada kullanılmış ve kullanılmaya devam etmektedir. Bu detektörler aynı zamanda hızlandırıcı tesislerinde ışın demeti kaybı ve güvenlik amaçlı olarak da kullanılabilmektedir.

Silikon PIN fotodiyotlar, özel bir dönüştürücü malzeme ile birlikte kullandıklarında nötron deteksiyonu için de uygundur. ^{10}B ve ^{6}LiF, termal nötron deteksiyonunda en sık kullanılan nötron-yüklü parçacık dönüştürücü malzemelerdir. Bu malzemeler termal nötronun absorbe edilmesinin ardından alfa ve triton ışımaları yaparlar. Bu parçacıklar ise Silikon PIN fotodiyotlarda kolayca detekte edilebilirler. Hızlı nötronların söz konusu olduğu durumda ise, polietilen yüksek hidrojen içeriği dolayısıyla en sık kullanılan dönüştürücü malzemedir. Hızlı nötronlar, polietilen içerisindeki hidrojenin tek protonunu, elastik çarpışma ile, polietilen molekülünden söküp dışarı atabilirler. Serbest hale geçen bu protonlar, daha sonra detektöre ulaştıklarında, Silikon içerisinde bıraktıkları enerji dolayısıyla deteksiyonları gerçekleşmiş olur.

Literatürdeki çalışmalara bakıldığında, farklı malzemelerde dahi, ikincil parçacık üretim ve absorbe olma oranları belli bir dönüştürücü kalınlığının üzerinde genellikle sabit kalmaktadır. Optimum kalınlık değerinin, birkaç yüz mikron olduğu görülmektedir.

Silikon PIN fotodiyot kullanılarak tasarlanan detektör sistemlerinin çoğunda, küçük yüzeyli ve tek bir fotodiyot kullanıldığı görülmektedir. Bu detektörlerin sinyal elektroniği ve kontrol birimleri de çoğunlukla ticari ve oldukça pahalı cihazlardan oluşmaktadır. Bu tez çalışmasında mevcut nötron deteksiyon sistemlerine alternatif, tüm elektronik ve kontrol birimlerini barındıran bir sistem geliştirilmiştir. Düşük maliyetli ve dokuz adet First Sensor firmasına ait PS100-CER-PIN2 model penceresiz Silikon PIN fotodiyot kullanılarak geliştirilen detektör, çeşitli hidrojen zengin dönüştürücü malzemelerle test edilmiştir.

Geliştirilen yeni nötron detektöründe herbir sensör elemanının kendine ait, bağımsız, bir sinyal okuma elektroniği bulunmaktadır. Bunlar son derece düşük gürültülü JFET temelli bir yük hassas ön yükseltici ve işlemsel yükseltici (Op-Amp) temelli bir şekillendirici yükselticiden oluşmaktadır. Ön yükseltici, doğrudan sensöre bağlı olan ilk yükseltme katmanıdır ve düşük gürültülü olması düşük enerjili protonların detekte edilebilmesi açısından oldukça önemlidir. Her sensör kanalından elde edilen sinyaller, bağımsız olarak işlenmektedir ve belli bir eşik değerinin üzerine çıkan sinyaller, yine her kanal bağımsız olmak üzere tek bitlik bir analog dijital çevirici devre elemanı yardımıyla dijitalize edilmektedir. Son olarak dijital sinyaller bir FPGA işlemcisi

yardımıyla, kullanıcı tarafından belirlenen süreler boyunca, birbirinden bağımsız olarak sayılmaktadır.

Dijital sinyallerin sayım işlemleri 100 MHz' lik saat sinyali ile çalıştırılan FPGA işlemcisi içerisinde tasarlanmış sistem ile gerçekleştirilmektedir. VHDL dilinde tasarlanan sistem, 10 ns gibi oldukça kısa zaman aralıklarında ve yüksek doğrulukta işlem yapabilme kapasitesine sahiptir.

Okuma sistemi beş alt birimden oluşmaktadır. Bunlardan en önemlisi her sensör (fotodiyot) kanalını birbirinden bağımsız okuyan ve sayım işlemini gerçekleştiren *Puls Sayıcı Modül*' dür. Altında dokuz ayrı sayıcı birim bulunan bu ana modül, bir çeşit arayüz görevi görmektedir ve alt birimlere giden kontrol bilgilerinin tek elden alınması ve tüm alt birimlere dağıtılması görevini gerçekleştirmektedir. Ayrıca sayım işlemi sona erdiğinde verilerin tek elde toplanması ve ilgili diğer bir modüle aktarılması süreci de yine burada kontrol edilmektedir.

En alt katmanda bulunan ve asıl sayım işlemini gerçekleştiren sayıcı birimler farklı sebeplerden kaynaklanabilecek hatalı sinyalleri saymamak için, özel olarak tasarlanmıştır. Bu amaçla her bir sayıcı birimin giriş kısmına bir kenar "detektörü" yerleştirilmiştir. Bu tür bir detektör, her saat vuruşu (clock cycle) için sinyal hattından örnekleme yapar ve okuduğu bu değeri bir önceki okuduğu değerle karşılaştırarak, gerçek sinyali hatalı sinyallerden ayırır. Bunu yaparken, gerçek sinyalleri, takip eden iki saat periyodunda, birbirinden farklı voltaj değerlerinde olması prensibinden yararlanmaktadır. Kenar detektörü bu farklılığı tespit ettiği anda bir kenar yakalamış ve gerçek sinyali belirlemiştir. Çünkü gerçek sinyallerin bir saat vuruşundan daha uzun olduğu bilgisi sensör hattından elde edilen dijital sinyaller kontrol edilerek belirlenmiştir. Hatalı sinyaller ise çoğunlukla, oldukça kısa süreli veya diğer bir tabirle yüksek frekanslı olmaktadır. Sinyal jeneratörüyle yapılan kontrollerde, sisteme verilen detektör çıkışına benzer bir sinyalin frekans değeriyle, elde edilen sayım sonucunun tutarlı olduğu açıkça gözlenmiştir. Sayıcılar 24-bit ($16x10^6$) sayım kapasiteli olarak tasarlanmışlardır. Yapılan testlerde 24-bit rezolüsyonun yeterli olduğu gözlenmiştir.

Tüm sistem, diğer bir ana modül olan ve ölçüm süresini kontrol eden zamanlayıcı modülün kontrolü altında sayım işlemlerini gerçekleştirmektedir. Bu modülde belirtilen süre boyunca sayım işlemleri devam etmekte ve süre dolduğunda buradan gelen bir sinyalle, sayım işlemi sonlandırılmaktadır. Ardından, her bir sayıcı alt biriminden elde edilen sayım verisi bir sonraki modüle, Raspberry Pi' ye aktarılıncaya kadar bekletileceği, veri düzenleme modülüne gönderilmektedir.

Veri düzenleme modülü, FPGA işlemcisi içerisinde tanımlanmış bir RAM bloğudur. Bu modül bağımsız sayıcılardan gelen 24-bit' lik sayım verilerininin sırasıyla analiz ortamına gönderilme sürecini yönetmektedir. Bu uygulamada görece standart bir iletişim protokolü olan seri hat kullanılmıştır. Bu hat üzerinde iletilebilecek maksimum veri büyüklüğü 8-bit ile sınırlı olduğundan, dokuz adet 24-bit' lik sayım verisinin herbiri 8' er bit' lik parçalara bölünerek Raspberry Pi' ye gönderilmesi gerekmektedir. Bu işlem de yine veri düzenleme modülü içerisinde gerçekleştirilmektedir. Ardından, veriler 8-bit' lik parçalar halinde iletişim sürecini yöneten UART modülüne sırasıyla aktarılarak, iletim işlemi gerçekleştirilmektedir.

Raspberry Pi ile FPGA arasındaki iletişimi yöneten UART modülü, 115200 bit/s' lik hızla çalışmak üzere tasarlanmıştır. Bu hız aynı zamanda UART hattıyla, FPGA' dan bağımsız olarak, ulaşılabilecek en yüksek iletim hızıdır.

UART modülü sadece verilerin Raspberry Pi' ye iletilmesini değil aynı zamanda Raspberry Pi' den gelen komut bilgilerinin FPGA' ya aktarılmasını da sağlamaktadır. Alınan bilgi daha sonra cihaz kontrol modülüne aktarılarak, ilgili komutlar işlenmekte ve yerine getirilmektedir.

Sistemin mevcut halinde üç tip komut tanımlanmıştır. Herbir komut bir ascii karakteri ile eşleştirilmiş, böylece 8-bit' lik bir iletişim yöntemi sağlanmıştır. Buna göre "A" karakterine karşılık gelen "01000001" baytı ölçüm başlatma, "B" karakterine karşılık gelen "01000010" baytı ölçümü durdurma ve "C" karakterine karşılık gelen "01000011" baytı da sistemin resetleme işlemi ile ilgili tanımlanmış komutlardır.

Bahsedilen komutların FPGA' ya gönderilmesi ya da FPGA' dan gelen ölçüm verilerinin anlamlı bilgilere dönüştürülmesi süreci, tamamıyla Raspberry Pi üzerinde gerçekleştirilmektedir. Bu süreç Python dilinde hazırlanmış grafik arayüzü bulunan bir programla yönetilmektedir. Buna göre belli butonlara basmak suretiyle, ilgili komutlar kolaylıkla FPGA' ya gönderilebilmekte ve sistemin işleyişi kontrol edilebilmektedir.

Raspberry Pi tarafında, FPGA' dan gelen ölçüm sonuçlarının alınması ve düzenlenmesi sırasında, program sürekli iletişim hattını dinleme durumunda beklemektedir. Veri alışveriş sürecinde iletişim hattının iki tarafı, tanımlanan özel bir bayt ile göreceli olarak senkronize edilmiştir. Buna göre program, gelen ilk baytın program içerisinde tanımlanan başlangıç baytı olup olmadığını kontrol eder. Ondalık olarak 127, binary olarak "01111111" şeklinde tanımlanan bu haberci bayt, ardından gelecek 27 baytlık sayım verisinin habercisidir. Program bu ilk baytı gördükten sonra, ardından gelen baytları üçerli bloklar halinde alarak toplam 9 blok veri alım süreci gerçekleştirmektedir. Herhangi bir sebepten ötürü olası hatalı bir 28. bayt gelmesine karşılık, bu süreç 27 bayt ile sınırlandırılmıştır. Yeni bir veri kabulu sadece en baştaki haberci baytın yeniden gelmesiyle mümkün olmaktadır.

Veri alım süreci bittikten sonra, her bir sensör kanalından elde edilen sayım değerleri, grafik arayüz ekranında, ilgili kanalın adını belirten kısımda sayısal, ikinci bir ekranda da grafik olarak gösterilmektedir. Burada gösterilen her veri, eş zamanlı olarak her kanal için ayrı olmak üzere bir metin dosyasına kaydedilmektedir.

FPGA temelli ölçüm sistemi, kompakt bir cihaz oluşturma adına görevini başarıyla yerine getirmektedir. Ancak detektörün daha detaylı testlerinin yapılması amacıyla, enerji spektrumlarının elde edilmesi için, bazı spektroskopik ölçümler yapılması öngörülmüştür. Bu amaçla mevcut şekillendirici yükseltici yerine, dokuz sensörden bir tanesi, Model 2020 NIM spektroskopi yükselticiye bağlanmıştır. Yükseltme oranlarının ve şekillendirme zaman sabitlerinin kolayca ayarlanabilmesi ve unipolar sinyal çıkışı vermesi, bu yükselticinin tercih edilmesinin nedenidir. Model 2020, sadece nötron deteksiyonu ile ilgili karşılaştırma ölçümlerinin değil, aynı zamanda gama ve alfa ışınlarıyla ilgili ölçümler yapılmasına da imkan vermiştir.

Spektroskopik ölçümlerden ilki ^{226}Ra kaynağının yaydığı alfa ışınlarının deteksiyonuna yöneliktir. Oluşan protonların Silikon malzeme içerisinde oluşturacakları sinyalin yüksekliği bilinmediğinden, enerjisi bilinen alfa kaynağı ile yapılan ölçümlerin, yükselticinin kazancının ayarlanmasında faydalı olacağı düşünülmüştür. Bu nedenle ^{226}Ra kaynağının alfa spektrumu alınmıştır.

Alfa kaynağıyla yapılan testlerin ardından gerçekleştirilen nötron ölçümlerinde, çevirici malzeme olarak farklı hidrojen zengin malzemeler kullanılmıştır. Sayım sistemi ve spektroskopi sistemiyle eş zamanlı gerçekleştirilen ölçümlerde, yüksek yoğunluklu polietilen, parafin, plexiglass, FR4 ve Silikon kullanılmıştır. Her iki sistemin ölçüm sonuçlarının belli bir eşik voltaj değerin üzerinde uyumlu sonuçlar verdiği görülmüş, dönüştürücü malzeme kullanılan ve kullanılmayan ölçümlerin birbirinden ayrıldığı belirlenmiştir.

Am-Be nötron kaynağında bulunan ^{241}Am' den, alfa parçacığının yanı sıra yayınlanan 59 keV' lik gama ışınının da gözlenmesi mümkün olmuştur. ^{241}Am, ^{152}Eu, ^{207}Bi, ^{137}Cs ve ^{60}Co kaynaklarını kullanarak yapılan ölçümlerde, nötron ölçümlerinde kullanılandan 10 kat daha yüksek bir yükseltme katsayısı kullanılması gerektiği belirlenmiştir. Gama ışınlarının düşük sinyal genlikleri dolayısıyla, nötron ölçümlerinde gürültü seviyesinin altında kalmaları nedeniyle sayımlara katkıları bulunmadığı gözlenmiştir.

Bu calışmada tasarımı yapılan ve prototipi üretilen bu tür bir detektör reaktörlerde hızlı nötronların akı tayini için, hızlandırıcı tesislerinde ya da nötron terapisi yapan sağlık merkezlerinde güvenlik amaçlı olarak kullanılabilir.

1. INTRODUCTION

Radiation detection devices have gained increasing importance especially in terms of national security in recent years. In particular, radiation detectors have become more efficient to detect radioactive materials in small quantities. Neutron detectors exist in various sizes to control border crossings to prevent radioactive material smuggling. Since in situ detection is often required, detectors providing accurate and instantaneous measurements are necessary for real-time monitoring.

1.1 Purpose and Scope of the Thesis

In this thesis study, we aimed to develop a new neutron detection system based on Silicon PIN photodiodes. In this manner, we first concentrated on the interaction mechanism of neutrons with matter. It is fact that the neutrons are uncharged particles, using bare Silicon as an active detector element is not useful. Thus, neutron to a charged particle converter materials were used to detect neutrons indirectly. Silicon PIN photodiodes were used as an active detector element because of their operational advantages, low cost and availability. Hence, we ensured to convert the neutrons to charged particles and detect these charged particles with Silicon PIN structure. At the end, a prototype neutron detection system was introduced. The complete electronic setup including a custom made charge sensitive preamplifier, shaping amplifier and control logic have been developed in this thesis.

1.2 Radiation Basics and Neutron Radiation

Radiation is any process that transmits energy through space or a material away from a source. In nuclear manner radiation consists of different types which includes electromagnetic radiation and particle radiation [21]. We can summarize the ones that we deal in this thesis work as follows;

- Alpha (α) Radiation

- Beta (β) Radiation
- Gamma (γ) and X Radiation
- Neutron Radiation

1.2.1 Alpha radiation

Alpha particle is the heaviest of all particle radiation types. It is mainly a Helium atom nucleus (^4_2He). Positive electric charge of alpha particle, makes it to interact with surrounding materials more than the above mentioned other radiation types. Thus, the mean free path of an alpha particle is much smaller than others. Additionally, inhaling or swallowing an alpha radiation source may result in serious health issues for sensitive human tissues like lungs. Radium, Radon, Uranium, Thorium are some of alpha emitter nuclides [21].

1.2.2 Beta radiation

Beta particle is also a charged particle radiation which consists of an ejected electron or a positron. This type of radiation has a longer range in the air compared to alpha radiation and more penetrating than alpha particles because of smaller charge and mass which cause less interaction with surrounding materials [21].

1.2.3 Gamma and X radiation

Gamma or X-Rays are highly penetrating electromagnetic radiations. These type of radiations can travel very long distances in air and also in materials. Thus, dense materials are necessary for shielding against gamma and X-rays. Additionally, gamma and X-rays usually accompany the emission of alpha and beta radiation during radioactive decay [21].

1.2.4 Neutron radiation

Neutrons are subatomic particles, shown with symbol " n " , and do not carry any electric charge. Neutrons constitute the nuclei of atoms together with protons within the nucleus. Each particle has approximately one atomic mass unit and they are both referred to as nucleons [21, 22].

In a similar way of electromagnetic radiation, neutrons are also classified depending on their energy ranges. The purpose of classification is to distinguish how neutrons interact with materials used for applications utilizing fission, such as nuclear power, weapons development, and isotope production. They are relevant for the discussion of biological effects from neutrons, as well, because how neutrons interact in the body depends on their energies. The main types of neutrons are thermal, epithermal, slow, fast and ultra fast neutrons.

Thermal neutrons are in equilibrium with the motion of the atoms that make up the medium in which they present. The most probable energy of thermal neutrons at 20° C is 0.025 eV.

Epithermal neutrons have energies between thermal (.025 eV) and 1 eV. They represent the transition region between thermal and slow neutrons.

Slow neutrons have energies between 1 eV to 1 keV.

Intermediate neutrons, as it is indicated in the name, have energies between slow and fast neutrons which is roughly 1 keV and 0.5 MeV.

Fast neutrons usually indicated with energies between 0.5 and 20 MeV. These are the energies of neutrons emitted by fission sources.

Ultra fast neutrons have energies above 20 MeV.

1.3 Neutron Radiation Sources

Neutron emitting radioactive sources are strictly limited. Neutron stars and the artificially made ^{252}Cf are the only ones. Moreover, neutron generators are available and they are widely used for many different applications.

1.3.1 Californium (^{252}Cf)

The only available, single element, neutron source is Californium and it is not exactly a natural radioisotope element. It was first produced by the bombardment of Curium with alpha particles in February 1950, at the University of California, Berkeley [23]. Among the known twenty isotopes, Californium-252 is the most commonly used neutron source, with a half-life of 2.64 years. One of the example use of Californium is to initiate nuclear reactors. It is also used for conducting research in the field of material science.

1.3.2 Radioisotope (α,n) sources

There are many artificial radioisotope neutron sources as shown in table 1.1 [1]. The main reaction, as shown in equation 1.1, states that an alpha radiation emission is followed by the absorption in Beryllium nucleus. The resulting Carbon atom is left in an excited state. Thus, a 4.44 MeV gamma photon is emitted to return the carbon atom back to a stable ground state.

$$\alpha \ + \ ^{9}Be \quad \rightarrow \quad ^{13*}C \quad \rightarrow \quad ^{12}C \ + \ n \ + \ \gamma \quad (4.4MeV) \qquad (1.1)$$

A J.L. Shepherd Model 179 Americium-Beryllium (^{241}Am-Be) neutron source (Figure 1.1) was used for our neutron based measurements. This Am-Be neutron source has 3 Ci activity. It is positioned in a large container with 1.2 m height and 1 m diameter. The shielding material is the combination of paraffin, lead and stainless steel.

Figure 1.1 : Photograph of 3 Ci Am-Be neutron source from J.L. Shepherd and Associates.

Table 1.1 : List of (α,n) radioisotope neutron generators [1].

Nuclide	Half-Life	E_α (MeV)	Yield per 10^6 alpha's ($n.s^{-1}$)	Yield ($n.s^{-1}.Ci$)	Yield ($n.s^{-1}.g^{-1}$)	Average Neutron Energy (MeV)
^{238}Pu	89 y	5.50	-	2.8x10^6	4.5x10^6	4.00
^{239}Pu	24.360 y	5.14	65	1.6x10^6	1.2x10^6	4.59
^{210}Po	138 d	5.30	73	2.5x10^6	1.1x10^6	4.54
^{241}Am	458 y	5.48	82	2.2x10^6	6.5x10^6	4.46
^{244}Cm	18.1 y	5.79	100	3.0x10^6	2.5x10^6	4.31
^{242}Cm	163 d	6.10	118	4.0x10^6	$\sim 10^6$	4.16
^{226}Ra	1620 y	7.69 to 4.77	502	1.1x10^6	1.5x10^6	3.94
^{227}Ac	22 y	7.36 to 5.65	702	1.5x10^6	1.7x10^6	3.87

1.3.3 Photoneutron sources

Unlike radioisotope neutron sources that emits at different energies, photo-neutron sources (or gamma neutron) result a mono energetic neutron emission just like the gamma sources [2]. Radioisotope gamma sources produce gamma rays mostly below 3 MeV. It is necessary to consider only the (γ, n) reactions in Beryllium (1.665 MeV threshold) and Deuterium (2.225 MeV threshold). The equation 1.2 shows the reaction in order to generate neutrons using high energy gamma rays from Beryllium atom.

$$^{9}Be \ + \ \gamma \quad \rightarrow \quad ^{8}Be \ + \ n \tag{1.2}$$

Only a few gamma ray sources, emitting above these threshold levels, exist with acceptable long half-lives. ^{124}Sb (60 day half life), ^{88}Y (107 day half-life) and ^{226}Ra (1600 year half-life) are the available sources in equilibrium with their daughters. The gamma rays emitted from these two sources are capable of producing neutrons only from Beryllium. The Radium source will generate photoneutrons from Deuterium as well. The characteristics of these two sources are given in table 1.2 [2].

Table 1.2 : Specifications of common photoneutron sources [2]

γ emitter	Half-Life	γ ray Energies (MeV)	Target	Average Neutron Energy (keV)	Neutron Yield n.s^{-1}Ci^{-1}
^{124}Sb	60 d	1.691		26	$\sim$ 5x10^{6}
		2.091	Be		
^{88}Y	107 d	1.836		200	3x10^{6}

1.3.4 Reactions with accelerated charged particles

In contrast to the natural or radioisotope based neutron generators, electronically controlled neutron sources have been developed with advancing accelerator technology. Such systems can be controlled with a computer user interface just like an X-ray source.

The operation principle of accelerator-type neutron sources are based on two main reactions in which isotopes of the hydrogen atom are used [24].

The latter is mainly due to Deuterium-Deuterium (D-D) reaction as shown in equation 1.3. The Deuterium atoms accelerated in a relatively strong electric field (several 100 kV) hit Deuterium target and produce free neutrons.

$$ {}^{2}_{1}H \;+\; {}^{2}_{1}H \quad\rightarrow\quad {}^{3}_{2}H \;+\; {}^{1}_{0}n \tag{1.3}$$

The second type of accelerator-based neutron generators work according to the Deuterium-Tritium reaction as shown in equation 1.4. Here again, the Deuterium atoms are accelerated in the same way as before, but this time the target material is Tritium [24].

$$ {}^{2}_{1}H \;+\; {}^{3}_{1}H \quad\rightarrow\quad {}^{4}_{2}He \;+\; {}^{1}_{0}n \tag{1.4}$$

Although the given examples to accelerator based neutron sources have common features like easy control and compact sizes (Figure 1.2), there are larger accelerator facilities which can provide high flux of spallation neutrons.

Figure 1.2 : The Photograph of Thermofisher MP320 Neutron Generator [3].

1.4 Interaction Mechanisms of Neutrons with Matter

Neutron interact via two main reaction mechanisms: scattering and absorption. Both types of interactions can occur at any energy, but in general scattering reactions dominate once the neutron energy is above a few hundred keV. Absorption can become significant especially at thermal and slow neutron energies. Thus they can be defined as follows [21,25,26],

- Scattering reactions
  - Elastic scattering
  - Inelastic scattering
- Absorption reactions
  - Capture reactions
  - Fission reactions
- Charged particle ejection reactions

1.4.1 Scattering reactions

In a scattering interaction, the neutron remains free after the interaction, but loses energy by transferring some energy to the nucleus it strikes. There are two types of scattering reactions: elastic and inelastic scattering.

1.4.1.1 Elastic scattering

In an elastic scattering interaction, the neutron shares its initial kinetic energy with the target nucleus, which emits recoil particle and keeps its initial state after the interaction [25, 26]. The interaction can be given as follows,

$$n + {}^{A}_{Z}X \rightarrow n + {}^{A}_{Z}X \tag{1.5}$$

The elastic scattering conserves both momentum and kinetic energy of the "system". It may be modeled as a billiard ball collision between a neutron and a nucleus. Figure 1.3 shows the schematic view of the elastic scattering of neutrons.

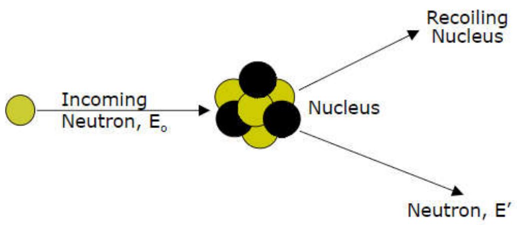

Figure 1.3 : Elastic scattering of neutrons as a schematic view.

1.4.1.2 Inelastic scattering

Inelastic scattering of neutrons is schematically shown in figure 1.4. Some energy of the incident neutron is absorbed by the recoil nucleus and the nucleus remains in an excited state in an inelastic scattering reaction between a neutron and a target nucleus [25, 26]. While momentum is conserved in an inelastic collision, kinetic energy of the "system" is not conserved.

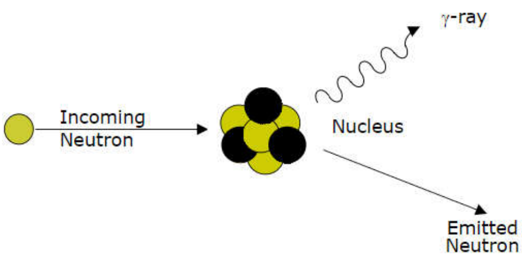

Figure 1.4 : Inelastic scattering of neutrons as a schematic view.

Inelastically scattered neutrons lose large fractions of their initial energy. The secondary radiation is produced as the target nucleus returns to its ground state. Inelastic scattering can be formulated as,

$$n + {}^{A}_{Z}X \rightarrow n' + {}^{A}_{Z}X' \rightarrow n' + {}^{A}_{Z}X + \gamma \qquad (1.6)$$

1.4.2 Absorption reaction

The most important type of reaction that take place in a nuclear reactor is the neutron absorption reaction which means that the neutron is completely absorbed and a compound nucleus is formed. The decay mode of such a compound nucleus is completely irrelevant to the way the compound nucleus was formed. Thus, different types of radiation emissions and decay may occur when a neutron interact with a nucleus. Capture reaction and fission reactions are the most common absorption reactions as well as charged particle ejection reactions.

1.4.2.1 Capture reaction

The neutron capture is one of the possible reactions that may occur. The schematic of the reaction is shown in figure 1.5. In fact, it is the only possible absorption reaction for non-fissionable nuclei.

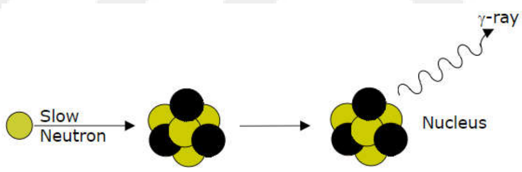

Figure 1.5 : Neutron capture reaction as a schematic view.

Capture reactions result in the disappearance of a neutron, coupled with the production of one or more gamma rays as shown in equation 1.7. This capture reaction is also referred as a radioactive capture or (n, γ) reaction [25, 26].

$$n + {}^{A}_{Z}X \rightarrow {}^{A+1}_{Z}X + \gamma \qquad (1.7)$$

1.4.2.2 Fission reaction

Some of the atomic nuclei present in nature are more susceptible to the fragmentation and split into smaller nuclei when exposed to neutron as shown in figure 1.6. In this event, which is known as the nuclear fission, two product nuclei as well as one or more neutrons are produced on average as shown in equation 1.8. Th, U, Np and Pu are the most common nuclei where the fission phenomenon is observed [25, 26]. In addition, nuclear fission reaction can occur in all neutron energies depending on the target nuclei which has a property of fission.

$$ {}_{0}^{1}n \; + \; {}_{Z}^{A}X \quad \rightarrow \quad {}_{Z'}^{A'}Y \; + \; {}_{Z"}^{A"}K \; + \; 3{}_{0}^{1}n \tag{1.8} $$

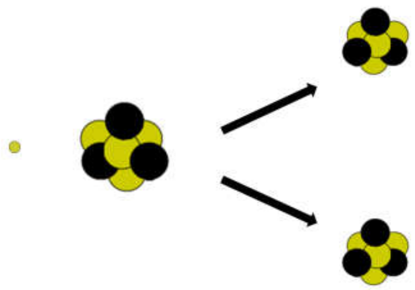

Figure 1.6 : Fission reaction as a schematic view.

1.4.2.3 Charged particle ejection reaction

These type of reactions are mostly related to formation of a new compound nucleus which ejects a charged particle while the incident neutron is kept inside the nucleus. Upon ejection of the new particle, the remaining nucleus is completely changed and it may not stay in an excited state. This is not a very common reaction type but it has an importance for the detection of neutrons.

The detection of all types of radiations is usually based on the ionization in an active sensor material. Following section provide basic information about the detection of radiation.

1.5 Radiation Detection Basics

When we deal with the radiation detection instrumentation, there are three types of detectors that are most commonly used depending on the specific needs [26,27]. These are:

- Gas-Filled Detectors
- Scintillator Detectors
- Solid State Detectors

1.5.1 Gas filled detectors

The first type of radiation detector, gas-filled detectors which is schematically shown in figure 1.7, are the most commonly used radiation detectors. There are several types of gas-filled detectors and they are all based on similar principles. However, they have many differences depending on operation characteristics. Basically when the gas in the detector comes in contact with radiation, the gas becomes ionized and the resulting electronic charge is measured by a meter [26, 27].

Ionization chambers, proportional counters, and Geiger-Mueller (G-M) tubes are the different types of gas-filled detectors. The main difference between these detectors is the applied voltage across the detector, which determines the type of response. Internal view of a usual gas filled detector is shown in figure 1.7.

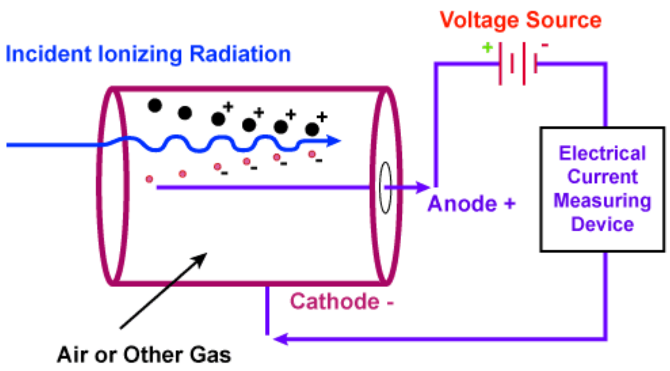

Figure 1.7 : A schematic view of a gas filled radiation detector [4].

1.5.2 Scintillator detectors

The second major type of detectors used for radiation detection is scintillation detectors. Each photon of radiation that interacts with the scintillator material (Figure 1.8) will result in a distinct flash of light. By that way, in addition to having high sensitivity, scintillation detectors are able to capture spectroscopic profiles for the measured radioactive materials [26, 27].

As shown in figure 1.9 scintillation detectors are operated with the connection of a scintillator material and a photomultiplier (PM) tube. The PM tube uses a photocathode material to convert each detected light into electrons and then amplifies the signal significantly in order to generate a voltage pulse with an acceptable amplitude. The number of these detected photons that are measured over time indicate the strength of the radioactive source being measured. However, the data for specific energy of the radiation together with the number of photons gives information on the type of radioactive material present.

Figure 1.8 : Plastic Scintillators in different shapes [5].

Scintillation detectors are particularly useful for radiation security applications due to their high sensitivity and potential ability to identify radioactive sources (resolution). Hand-held devices used for screening the containers and the monitors used for inspecting larger fields or populations are able to inspect natural or medical sources of radiation. Detecting of special Nuclear Materials (SNM) can also be counted as one of the applications of scintillator detectors.

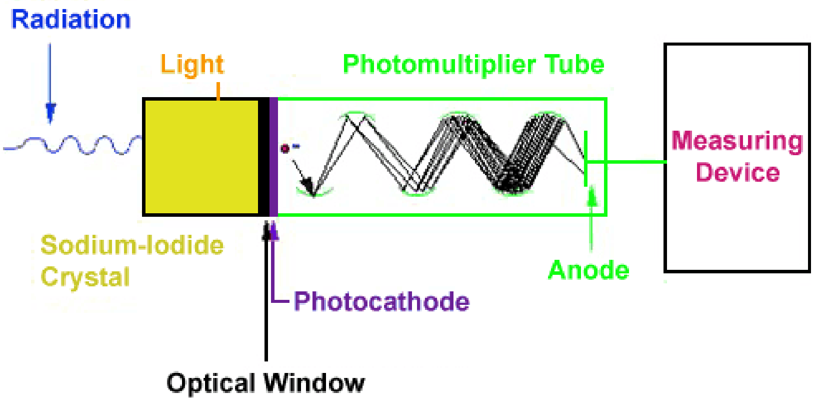

Figure 1.9 : Scintilator detector setup overall view - scintillator material (Sodium-Iodide Crystal) mounted on a photomultipler tube [6].

1.5.3 Solid state detectors

Solid state detectors are another widely used technology in radiation detection instruments. A semiconductor material such as Silicon operates much like an ion chamber, simply at a much smaller scale and at a much lower voltage. Semiconductors are the materials that have a high resistance to electronic current, but not as high resistance as an insulator. They are made up of lattice of atoms that contain "*charge carriers*" which are either electrons or electron "holes," (Figure 1.10) [26, 27].

Silicon solid state detectors are composed of two layers of Silicon semiconductor material, one "N-type" containing a greater number of electrons and one "P-type" having a greater number of holes. Electrons from the N-type migrate across the junction between the two layers to fill the holes in the P-type, creating what' s called a depletion zone.

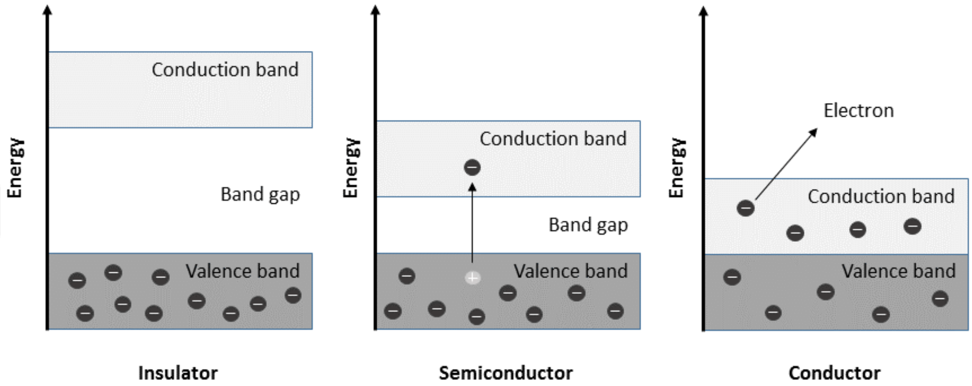

Figure 1.10 : Semiconductor band structure showing the valance and conduction bands and also the gap between these two bands [7].

This depletion zone acts like the detection area of an ion chamber. Radiation interacting with the atoms inside the depletion zone causes them to ionize and generate an electronic pulse which can be measured. The small scale of the detector and the depletion zone itself means that the ion pairs can be collected quickly by means the bias voltage applied to the semiconductor. The instrumentation utilizing this type of detector can have a particularly quick response time. With their small size, this type of solid state detectors are very useful for electronic dosimeter applications. They are also able to withstand a much higher radiation dose over their lifetime compared to other detector types such as G-M tubes. Thus, they are useful for instruments operating in the fields with high radiation levels.

1.5.3.1 Silicon PIN photodiodes

A photodiode has a very similar structure as usual PN junction diodes which uses voltage as the energy source for generating electric current whereas PIN (P-Intrinsic-N) photodiodes use voltage and light together for generating electric current. Thus, photodiodes are also referred as photo-detector, photo-sensor or light detector.

However, researchers have started using the photodiodes for non-photon (α, β) or high energetic photon, like γ radiation, detection purposes for a few decades.

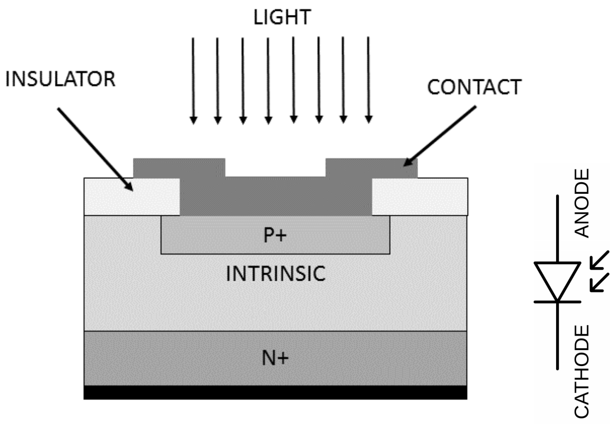

Figure 1.11 : Internal structure of a Silicon PIN photodiode (left) and the schematic representation of a Silicon PIN photodiode (right) [8].

Layers of PIN photodiode:

A PIN photodiode consists of three layers namely P-type, N-type and intrinsic semiconductors.The intrinsic semiconductor is located between the P and N type semiconductors to increase the current.

P-type semiconductor: In P-type semiconductors, the number of free electrons in the conduction band is lesser than the number of holes in the valence band. Therefore, holes are the majority charge carriers and free electrons are the minority charge carriers. In P-type semiconductors, holes carry most of the electric current.

N-type semiconductor: In N-type semiconductors, the number of free electrons in the conduction band is greater than the number of holes in the valence band. Therefore, free electrons are the majority charge carriers and holes are the minority charge carriers. In N-type semiconductors, free electrons carry most of the electric current.

Intrinsic semiconductor: In intrinsic semiconductor, the number of free electrons in the conduction band is equal to the number of holes in the valence band. Therefore, intrinsic semiconductor has zero net charge carriers to conduct electric current.

PIN photodiode operation:

Under reverse bias condition as shown in figure 1.12, the majority charge carriers in N region moves away from the junction. As a result, the width of depletion region becomes wider. Therefore, majority carriers will not carry electric current under reverse bias condition However, the minority carriers will carry electric current because they experience repulsive force from the external electric field.

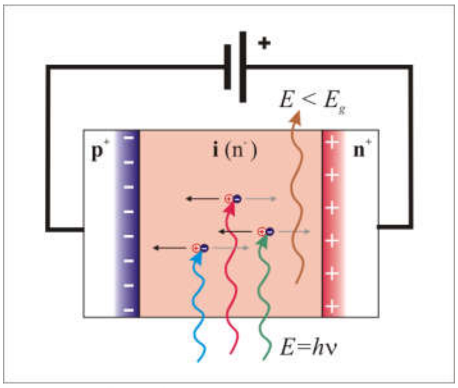

Figure 1.12 : Silicon PIN phtodiode reverse bias connection.

When radiation is in the PIN photodiode, some part of its energy is absorbed in the intrinsic or depletion region because of wider depletion width. As a result, a large number of electron-hole pairs are generated. Free electrons move towards n-side in contrast to the holes that move towards p-side (Figure 1.12). When free electrons and holes reach n region and p regions respectively, they are attracted to the positive and negative terminals of the power source.

The capacitance is directly proportional to the size of the electrodes and inversely proportional to the distance between electrodes. In PIN photodiode, the p region and n region acts as electrodes and intrinsic region acts as dielectric. The larger separation distance between p region and n region results in low terminal capacitance in a PIN photodiode.

1.5.3.2 Photodiodes operation modes

A photodiode can be operated in one of the two modes, photovoltaic mode or photoconductive mode as shown in figure (1.13). Operation mode selection of the photodiode depends upon the speed requirements of the application and the amount of dark current that is tolerable [28].

Photovoltaic mode:

In the photovoltaic mode, the photodiode is unbiased which means no external voltage is applied to the photodiode which results very low dark current. However, photodiodes operated in photovoltaic mode have low response speed. Thus this mode is generally used for low speed applications or for detecting low DC light levels.

Photoconductive mode:

In photoconductive mode, an external reverse bias voltage is applied to the photodiode. The reverse bias application increases the width of depletion region and reduces the junction capacitance which results in increased response speed. The reverse bias also increases the dark current. Photodiodes operated in photoconductive mode has high noise current. This is due to the reverse saturation current flowing through the photodiode.

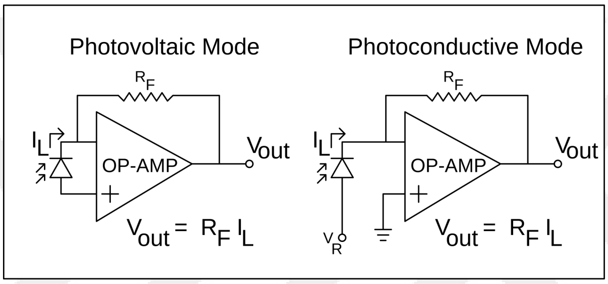

Figure 1.13 : Schematics of Photovoltaic and Photoconductive operation modes of Silicon PIN photodiodes [9].

1.5.4 Neutron detection using Si PIN photodiode based neutron detectors

One of the most important parameters of neutron detection is the converter material when Silicon PIN photodiodes are used as an active element. Although the secondary particle generation efficiency of these converter materials are low, there are available studies in literature for improving the production efficiency. Most of the available studies are based on crystal coupled photon detectors [10, 11, 29–32] and ^{6}Li or ^{10}B based alpha particle detection are also available [12, 13, 33–35]. Other examples are based on proton detection where hydrogen-rich materials such as polyethylene and paraffin are used [13, 14, 36].

1.5.5 Crystal as a neutron to photon converter

Detectors with scintillating crystals are mostly used for detection of thermal neutrons. This type of designs are based on the reaction between neutrons and scintillating material which results in high energy (mostly in MeV range) gamma emission [10, 11, 29]. An example study shown in figure 1.14 uses a LiI(Eu) crystal with double detectors mount on opposite sides of the crystal. Their purpose was to remove the noise by using the coincidence of two signals and the results seem to be acceptable to identify the peak (Figure 1.14) induced by the thermal neutrons.

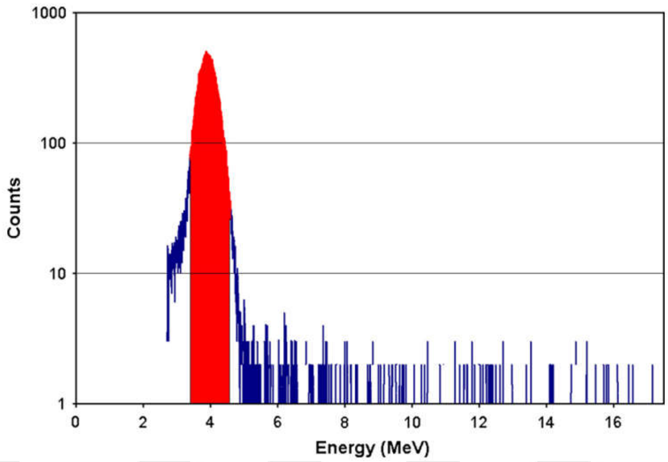

Figure 1.14 : The spectrum of ^{252}Cf neutron source [10].

In another study shown in figure 1.15, the researchers used CsI(Tl) crystal to identify the nitrogen by detecting characteristic gamma photons emitted after the activation by thermal neutrons [11]. This way, they aimed to detect possible explosive materials. The author claims that the method is adequate for this purpose.

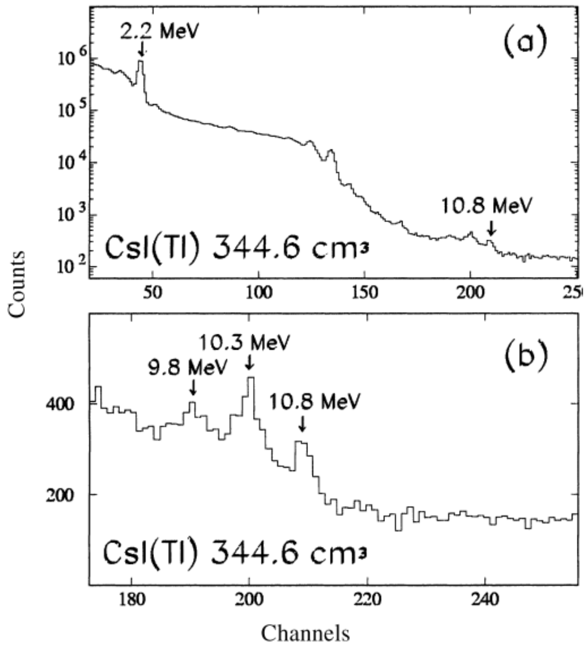

Figure 1.15 : Gamma spectrum obtained by irradiation of 800 g Melamine sample: The spectrum displayed on a logarithmic scale (upper); Region of interest around 11 MeV(lower) [11].

1.5.6 ^{6}LiF as a neutron to triton (^{3}H) converter

Although most of the studies for thermal neutron detection are based on the scintillation process, there are some other studies like the ones using a converter material. An example of these was published in 2003 [12]. In this study, researchers used ^{6}LiF as converter material, resulting the emission of triton (^{3}H) and alpha particles after the absorption of neutrons (Figure 1.16).

1.5.7 Polyethylene as a neutron to proton converter

Another popular method for detecting fast neutrons is the use of polyethylene (PE) layers as converter material. The high Hydrogen content of polyethylene $(C_2H_4)n$ makes this possible since the Q value (energy transferred to the nucleus) of the reaction increases with the increasing neutron energy and decreasing atomic number of the target material or nuclei. This reaction results in liberated recoil protons (Hydrogen nuclei) which are later to be detected by the photodiodes [13, 14, 36]. This method is suitable for the detection of fast neutron since it needs to break the nuclear bonds. The spectra shown in figure 1.17 was obtained with ^{252}Cf source.

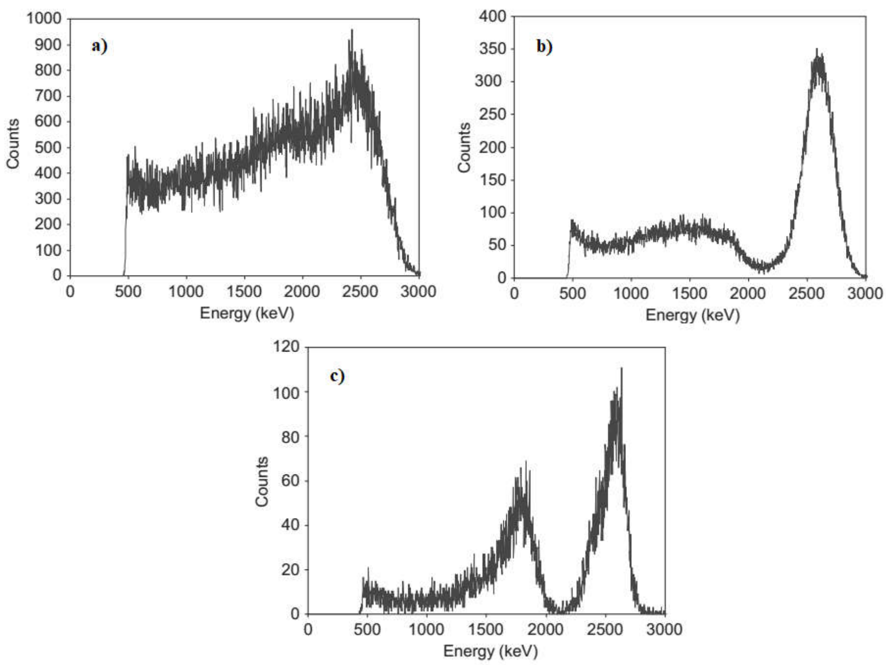

Figure 1.16 : The energy distribution of charged particles obtained with a) 300 μm, b) 2 μm and c) 0.6 μm ^{6}LiF-coated photodiodes; irradiated with neutrons below 10 MeV [12].

Although it is not as clear as in other applications, the results given in figure 1.16 shows that the neutrons from ^{252}Cf have been detected with PE layers (Figure 1.17). In addition to this, a much clear spectra has been recorded by another research group where the experiment was performed with an Am-Be neutron source (Figure 1.18).

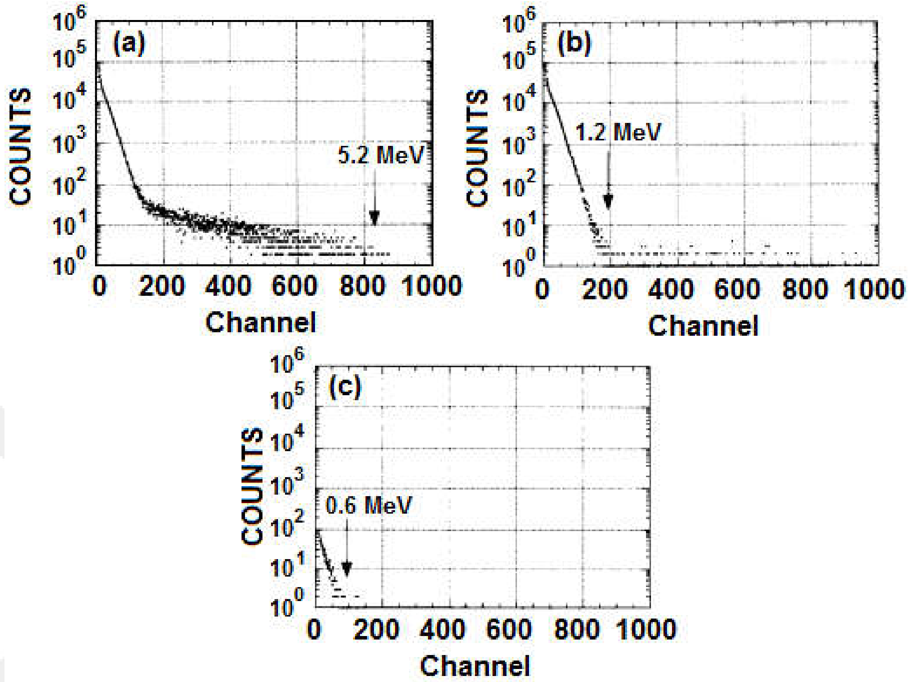

Figure 1.17 : The energy spectrum obtained using ^{252}Cf source and polyethylene converter a) 45μm polyethylene coating, b) No converter, c) Background [13].

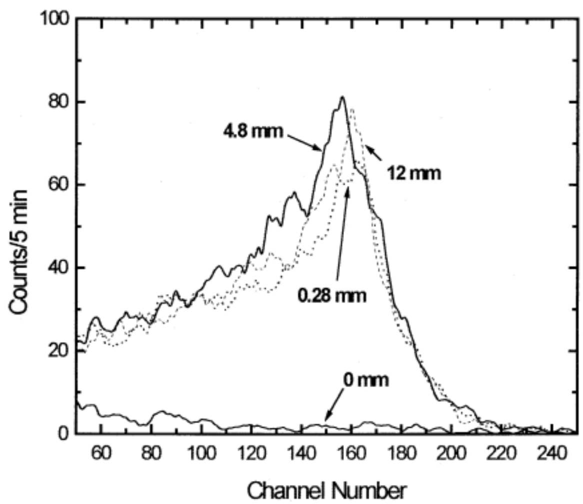

Figure 1.18 : Am-Be spectra of the Si-PIN photodiode with different polyethylene thicknesses and without the polyethylene converter [14].

2. DESIGN OF INSTRUMENTATION FOR NEUTRON DETECTION

In order to develop a complete radiation detection device, we followed common signal readout chain which is shown as a block diagram in figure 2.1. The signal readout chain consist of a sensitive sensor element which is connected to a bias voltage for charge collection from the sensor and then to a charge sensitive preamplifier (CSP) for first amplification. The signal shape of the output of CSP is in an exponential decay form with a relatively small amplitude. It is usually not capable of providing an information about the measured radiation. Thus, a second amplification is necessary. After this stage, the signal readout chain is divided into two separate links as shown in figure 2.1.

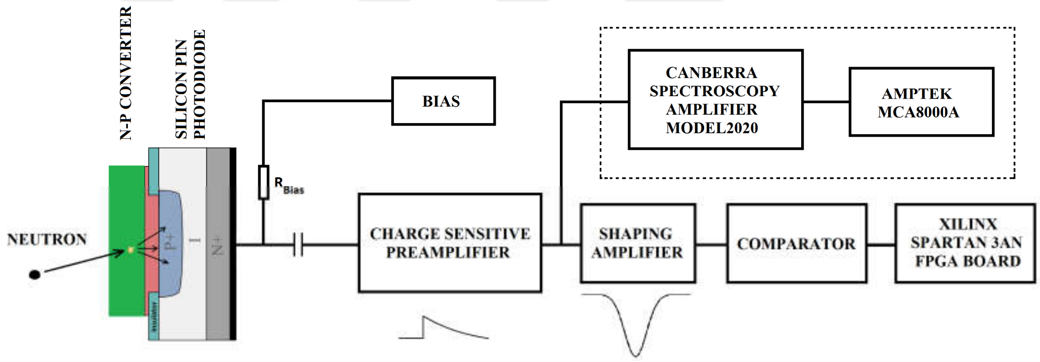

Figure 2.1 : Block diagram of the signal electronics.

First link is designed for the counting measurements and for the purpose of designing a complete device. Thus, following the charge sensitive preamplifier, a shaping amplifier or main amplifier stage is promoted. This circuit gives the final shape of the signal, could be chosen as a bipolar or uni-polar shape, with higher amplitude. After the shaping amplifier, the analog signal processing is finalized and a single bit digitizer performs the analog-digital conversion. At the end, an FPGA (Field Programmable Gate Array) controls the counting operation and transfer the results to the further analyzing environment which is a Raspberry PI for this system.

The second signal readout link shown in dashed lines in figure 2.1 is for spectroscopic measurements and it includes commercial standalone devices; a NIM (*Nuclear Instrumentation Module*) spectroscopy amplifier and a multi channel analyzer (MCA).

For the counting measurements, we used 9 individual Silicon PIN photodiodes for building a larger detection area. Also we connected 9 separate charge sensitive preamplifiers and shaping amplifiers including independent single bit digitizer integrated circuits for each photodiode. Therefore, the counter unit has 9 separate counter channels for each link. Additionally, the number of photodiodes can be increased depending on different applications in the future.

Using complete 9 individual channels has various advantages and disadvantages. There are applications connecting many photodiodes in parallel for increasing the active surface area; however, this results in an increased total capacitance of sensors which slows down the signal response [37]. This will cause loosing some signals. Conversely, using separate readout circuitry provides better signal processing. Also, in case of any damage on a particular channel, the user must be aware of that. Furthermore, each detector segment can be used for independent purposes if they are individually covered by different converter materials. Not to mention, this kind of segmented structure provides position information. This costs only little more complex circuit board structure.

In case of spectroscopic measurements, we used only one of the sensor channels by connecting one of the CSP output to the Canberra spectroscopy amplifier. This is followed by recording the spectra for different radiation sources and configurations on Amptek MCA.

As an extra element for the purpose of neutron detection, we used neutron to proton converter materials which are located just in front of the Silicon PIN photodiode active window.

2.1 Sensor Module

A relatively large detection area has been planned for increasing the detection efficiency. This is advantageous when the neutrons are coming from a large solid angle after scattering off the target. Thus, larger the detection area is better the detection efficiency. Depending on this, a sub-module of complete device named *Sensor Module* was designed by combining 9 individual Silicon PIN photodiodes in a matrix array form and including corresponding individual CSP for each photodiode.

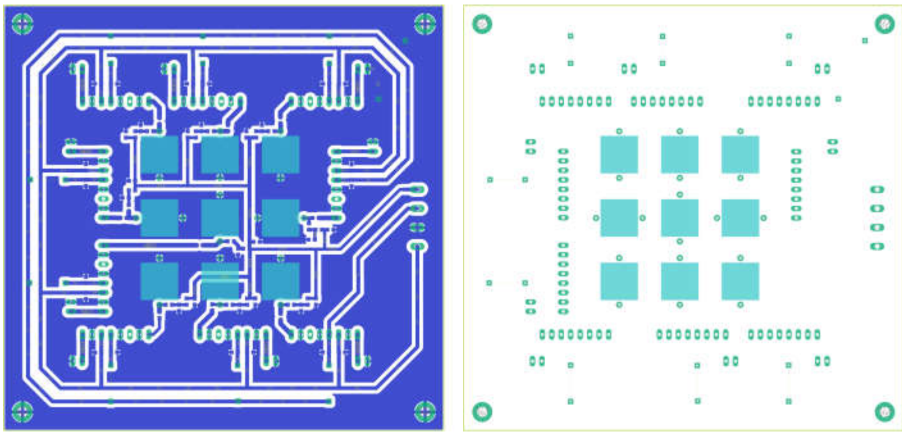

Figure 2.2 : The *Sensor Module* main board printed circuit board design. Bottom view on the left and top view on the right was prepared using CadSoft Eagle [15] electronic design software.

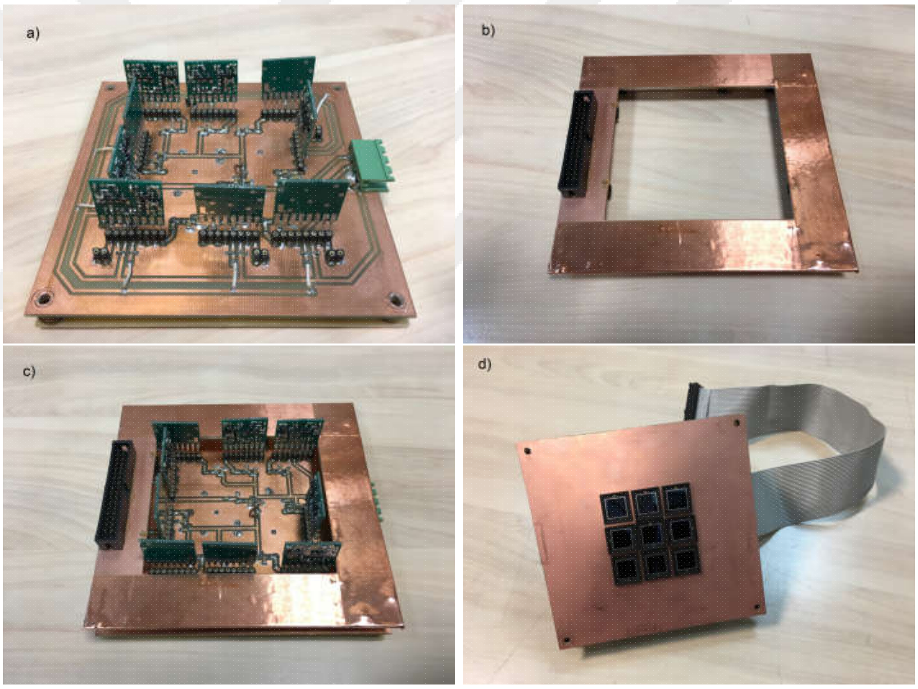

Figure 2.3 : (a) *Sensor Module* main board with connected CSPs. (b) *Sensor Module* frame board for carrying the signal paths in a suitable form. (c) Rear view of the *Sensor Module* final form. (d) Front view of the *Sensor Module* final form.

Main board of the *Sensor Module* has been designed on CadSoft Eagle [15] electronic design software as shown in figure 2.2 as a two layer PCB. The final version of the *Sensor Module* is shown in figure 2.3. Upper left picture shows the main board with connected CSPs. The frame in the upper right shows a sub-circuit which organizes the signal paths in a suitable form for transferring the them to the next stage. Rear view of the *Sensor Module* final form is shown in the lower left picture and lower right is the front view of the *Sensor Module* with connected 9 Silicon PIN photodiodes.

2.1.1 Silicon PIN photodiode

For neutron detection we used a relatively large area, 1 cm^2, Silicon PIN photodiode produced by First Sensor (Pacific Sensor) with model number PS100-7-CER-PIN-2 [16]. This windowless type photodiode is a good fit for our neutron detection purpose since we aimed to detect protons, converted from neutrons using a proton reach material.

Figure 2.4 : First Sensor PS100-CER-PIN-2 photodiode [16].

2.1.2 Bias potential

As stated before in chapter 1, to be able to collect the generated free electrons inside the radiation sensor, we need to generate an electric field which will carry these electrons to the amplifier input.

For our case as shown in figure 2.5, we applied reverse bias to the photodiode. This reverse bias will extend the *Intrinsic* region which will increase the detection volume in the photodiode and reduces the terminal capacitance thereby increasing the bandwidth. Applied positive potential is set to +6V because of its availability in our power supply. A detailed study for inspecting the effect of bias voltage on the detection efficiency was performed previously [38]. +50V the maximum value recommended by the manufacturer [16].

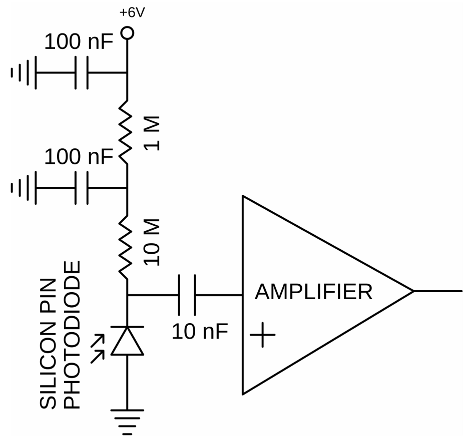

Figure 2.5 : Bias circuit schematics of the Silicon PIN photodiode signal readout.

2.1.3 Charge sensitive preamplifier - CSP

The first element on the signal path is a preamplifier. The preamplifier collects the charge produced within the sensor. In contrast with its name, a preamplifier is not exactly an amplifier but behaves like an interface between radiation sensor and pulse processing electronics. Signal extraction from the detector is the main function of a preamplifier without significantly changing the signal-to-noise ratio. Thus, the preamplifier must be located as close as possible to the sensor for eliminating the external noise may distort the signal.

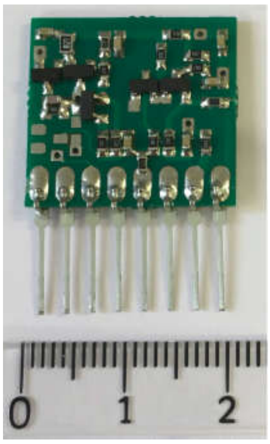

Figure 2.6 : Charge sensitive preamplifier circuit board.

For this project, we used the same charge sensitive preamplifier that we used for one of our previous group projects in order to develop an X-Ray imaging device [39] for industrial purpose. Here, low noise amplifiers were needed. The neutron detectors also need low noise amplifiers to detect the charged particles generated by the neutrons.

Figure 2.6 shows the photograph of the charge sensitive preamplifier used in this project.

2.2 Main Amplifier and Digitizer Module

Signal follows path through the photodiode, the charge sensitive preamplifier, the shaping amplifier and the discriminator, respectively. Since nine independent channels take place in the design, the main amplifier is built for combining the nine shaping amplifiers including the digitizers as shown in figure 2.7.

This unit is combined with the Xilinx FPGA board which is directly connected to the main amplifier module to reduce the extra cabling.

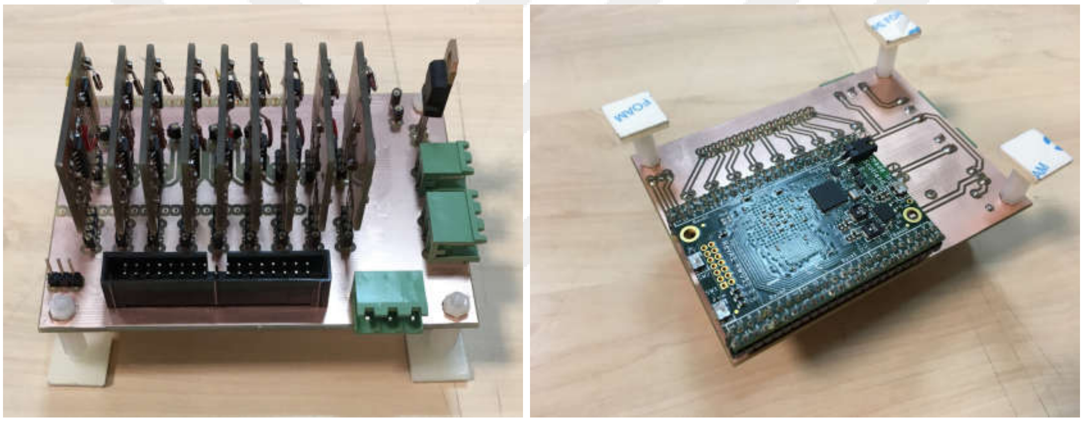

Figure 2.7 : a) Main amplifier unit including the shaping amplifiers. b) FPGA board connected directly to the main amplifier unit.

2.2.1 Shaping amplifier

The signal output of the charge sensitive preamplifier is not large enough for further processing, as mentioned before. A further amplification is necessary and it is achieved by using a separate amplifier board called shaping amplifier. Shaping amplifier board, as shown in figure 2.8, give the final shape of the amplified signal. This is a basic approach for the signal amplification which is known as active band pass filter. It has been known that PCB can be designed with many alternative options and parasitic capacitances can change the signal height in each design. For that reason, we have determined the optimum R and C values by trial and error instead of using detailed circuit simulations. As it is shown in figure 2.9, an example signal has approximately

10 μs width. The gain of the amplification was arranged to have 5V peak to peak signal amplitude at most. The baseline was 2.5V for the bipolar signal.

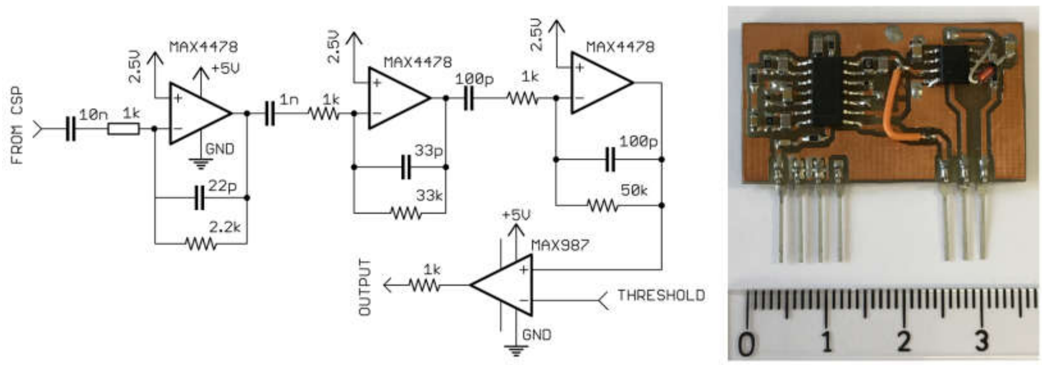

Figure 2.8 : Schematics of the shaping amplifier and the circuit board.

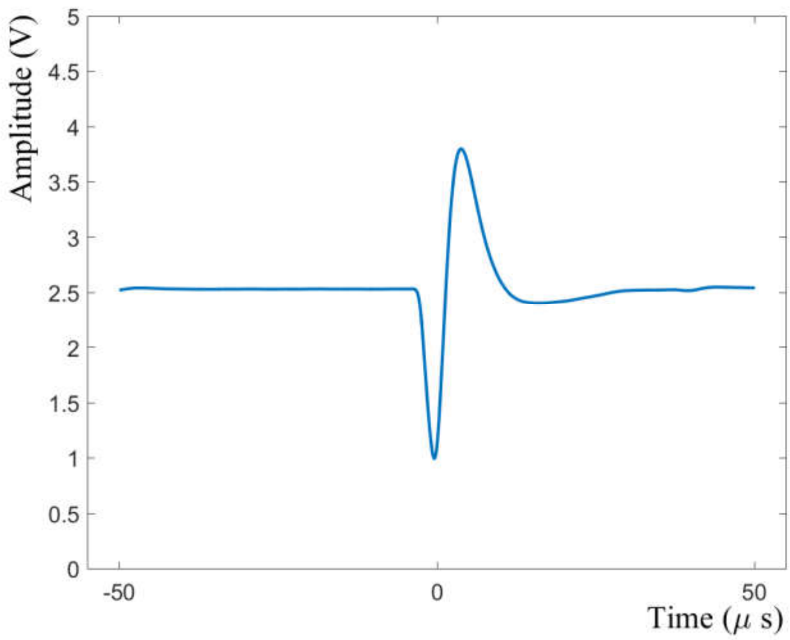

Figure 2.9 : Signal output of one channel from ^{226}Ra source.

2.2.2 Single bit digitizer

Following the signal shaping circuitry, a signal discrimination is applied to generate logic pulses for counting purposes. Here, we made use of a single bit digitizer (or a comparator) integrated circuit (IC) from Maxim Integrated Company, MAX987 [40].

As it is shown in figure 2.8, MAX987 has been connected to the final stage output of the 3 stage shaping amplifier circuit together with a variable threshold option. The applied threshold potential is adjusted through a variable resistor located on the side of the detector box.

Although the noise level is determined to be 100 mV conservatively, shaping amplifier and digitizer have been located on the same board to have the shortest possible signal path providing better signal to noise ratio. This design procedure was promoted a more compact design as shown in figure 2.8 on the right.

2.3 Multi Channel Counting System

So far the 9 channel analog and digital signal readout electronics explained in detail. After this point, having the digital signals from the digitizer IC, the next step is transferring these digital signals to a counter system. Thus, we needed a multi channel counting system which must perform individual counting for each sensor channel. For this purpose, there are microprocessor based development boards. We decided to use an FPGA (*Field Programmable Gate Array*) platform because of their high speed and reliable operations as well as their widely use in nuclear/particle physics experiments.

2.3.1 Field programmable gate array - FPGA

FPGAs are known as re-configurable integrated circuits meaning that it is possible to design a digital circuit inside an FPGA (Figure 2.10). ASIC (*Application Specific Integrated Circuit*) design is the main application area of FPGAs. Because unlike an ASIC the circuit design on an FPGA chip is not static and always there is an option to modify it.

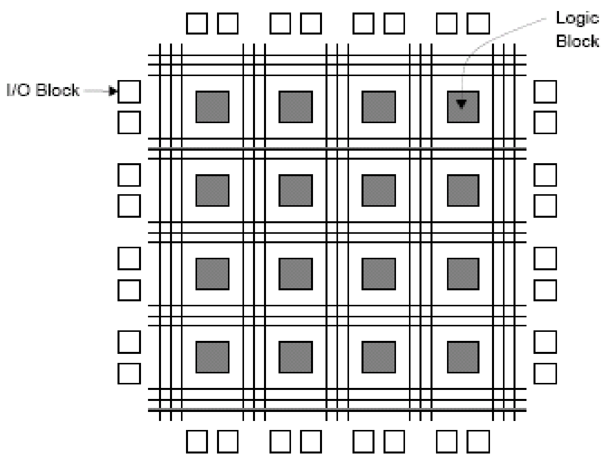

Figure 2.10 : Internal structure of an FPGA chip [17].

FPGAs are usually confused with microcontrollers. However, they are completely different platforms. In a microcontroller, user write a software and load it to a predefined hardware. Hence, in a processor, it is not possible to modify the hardware. Thus, they are controllable over the software. However, in FPGAs, user designs a digital circuit and there is no processor to run the software in it. To create a circuit, one must use one of the hardware description languages (HDL). VHDL (*Very High–Speed Integrated Circuit Hardware Description Language*) and Verilog are the two most popular HDLs. FPGA designs in this thesis study have been prepared using VHDL.

2.3.2 AES220B FPGA board

For this thesis work, we used a Xilinx Spartan 3AN family XC3S400AN FPGA chip on AES220B FPGA board from Aessent Technology (Figure 2.11) [18]. This board is advertised as credit card size FPGA board ant it fits our compact design goal. The board includes its own DC/DC converter and crystal oscillator. While the board can be powered through a USB drive, an external 5V DC power supply can be used as well.

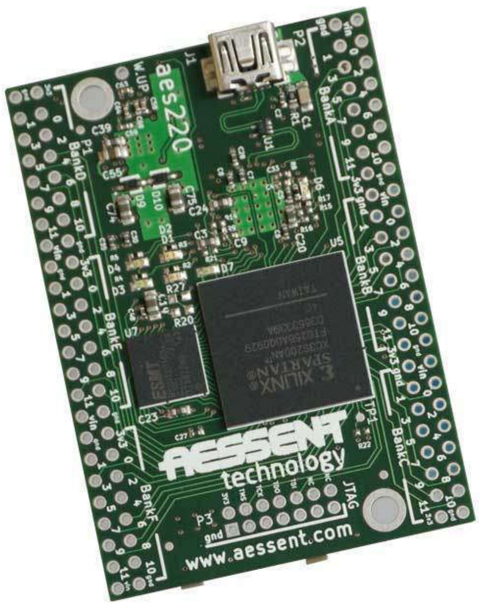

Figure 2.11 : AES220B Spartan 3AN FPGA board from Aessent Technology [18].

There are 72 GPIO ports for data readout and 4 clock managers which allows to adjust the clock frequency up to 334 MHz. In addition the SDRAM, device provides 128 MB of RAM memory with fast access time (16 bits parallel data bus and 100 MHz clock).

2.3.3 Xilinx ISE design suite

Xilinx ISE (*Integrated Synthesis Environment*) is a software tool (figure 2.12) produced by Xilinx for synthesis and analysis of HDL designs, enabling the developer to synthesize their designs, perform timing analysis, simulate a design's reaction to different inputs and configure the target device with the programmer [41]. Xilinx ISE is also a design environment for FPGA products from Xilinx, and it is coupled to the architecture of such chips. It can not be used with FPGA products from other manufacturers. The Xilinx ISE is primarily used for circuit synthesis and design while ISIM or the ModelSim logic simulator is used for system-level testing.

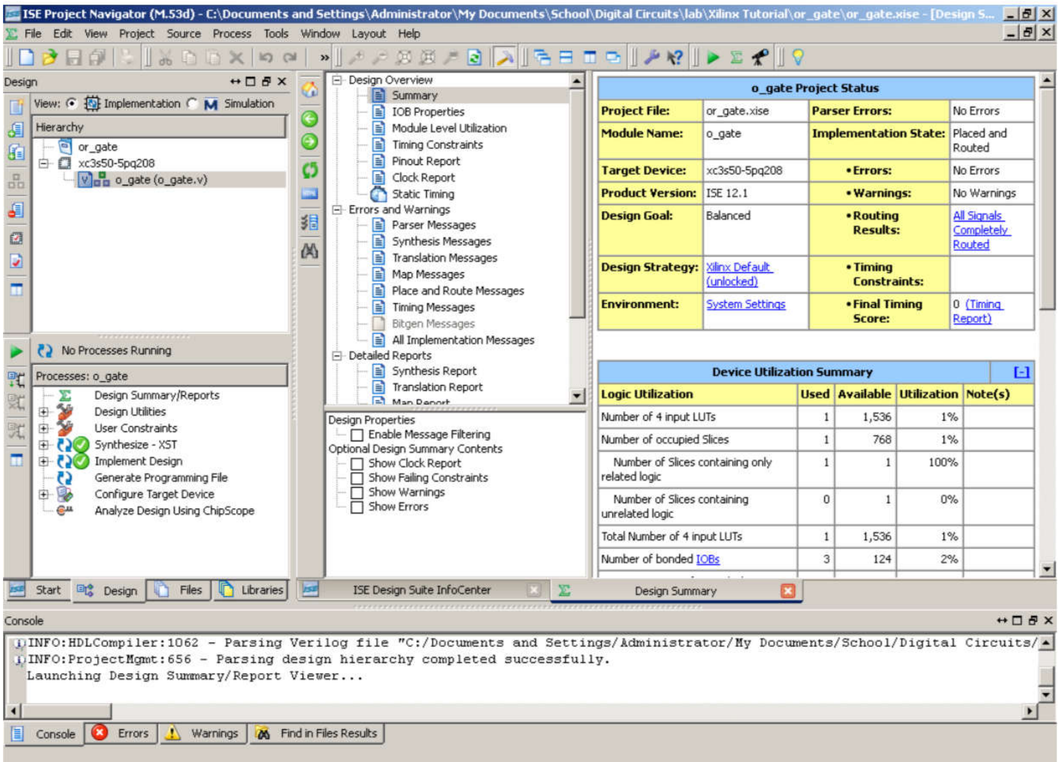

Figure 2.12 : Xilinx ISE Design Suite 14.7 project navigator.

2.3.4 Structure of FPGA counting system

The structure of the 9-Channel counting system is shown in Figure 2.13 as a block diagram. FPGA technology let us to read each sensor channel independently and fast. This system runs with 100 MHz clock speed meaning that each channel is read in 10 ns time periods.

As stated in the block diagram (2.13), there are 5 main sub-modules composing the 9-Channel counting system:

- *Stop Watch Module*
- *Pulse Counter Module*
- *Data Organizer Module*
- *UART Module*
- *Device Controller Module*

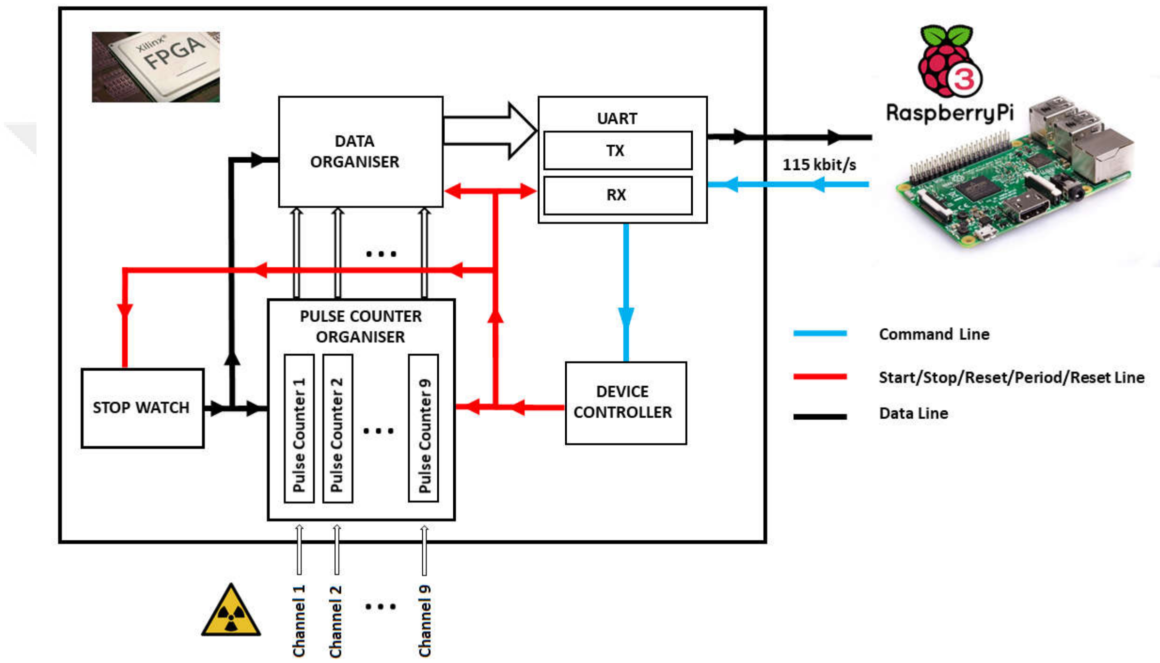

Figure 2.13 : Block diagram of FPGA multi channel counter design.

2.3.4.1 Stopwatch module

The timing control of the system is performed by the *Stopwatch Module*. This module is basically a clock counter. For instance, to be able to run a process in 1 second intervals, it is necessary to count up to $100x10^6$ if the clock frequency is set to 100 MHz. In case of larger time periods are need, nested counter blocks provide a simple solution. For instance, if a 10 minutes counting period is required, one can simply count the seconds up to 600.

2.3.4.2 Pulse counter module

Counter systems are clearly the main units in a counting measurement system. Thus, we care about this part specially. The *Pulse Counter Module* has been built around two parts. The first one is the real counter unit, performing the counting operation. The second one is an organizer, the outer module which receives the resulting count values from counter sub-modules at the end of each measurement period.

Counter units, as a feature of FPGA technology mentioned before, has the ability of operating independently since they are designed as separate units. This means that they can read the corresponding input port independent from the others. Thus, when a digital pulse received by one of the counters, this digital pulse is first processed by so called "*Edge Detector*". This part of the design performs a check whether the incoming pulse is real or fake and also prevents to count the same pulse more than once.

Edge Detector

The operation principle of an *Edge Detector* depends on the identification of a rising edge of a pulse signal which goes from logic 0 to 1. Thus, the edge detection circuit performs this check by comparing the signal on the link continuously at least for two following clock cycles. As an example, 2 step configuration uses the logic equation 2.1.

$$Egde\ \ Detector\ \ Output = NOT(signal^{1st})\ \ AND\ \ signal^{2nd} \tag{2.1}$$

As a result of the operation performed in equation 2.1, table 2.1 shows the possible outputs of a 2 stage edge detector. Depending on this, the signal level on the link must be in the first option to be able to state it as a real detector signal.

Table 2.1 : Two step edge detector output configurations.

1^{st} clock cycle	2^{nd} clock cycle	Result
LOW	HIGH	HIGH
LOW	LOW	LOW
HIGH	LOW	LOW

At the end of edge detection process, after a real signal is received by the counter, the register recording the count value is incremented by one and eventually a cycle of counting process is concluded. Each one of 9 pulse counters are capable of counting up to 24 Bits which correspond to a value close to 10^7. This is fairly large enough amount for our measurements.

2.3.4.3 Data organizer module

At the end of each measurement period, the resulting count data is delivered to the *Data Organizer* module for temporary storage. The structure of data organizer is based on a RAM block memory. 9 rows of 24 Bits wide RAM memory block has been reserved for this purpose (figure 2.14). Once the *Data Organizer Module* receives the data, it immediately starts transferring it to the UART module for transmitting to the analysis environment.

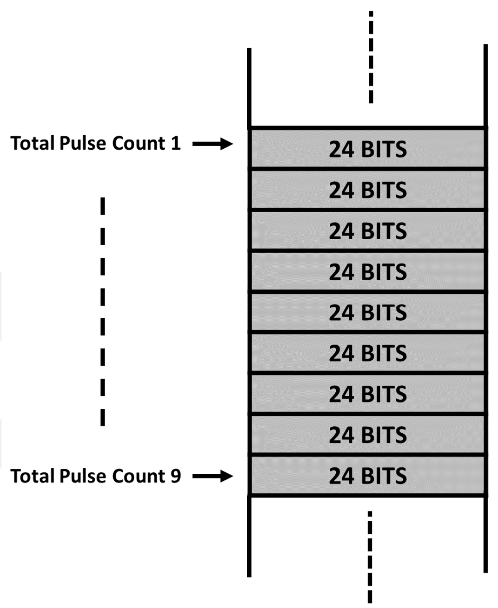

Figure 2.14 : Data Organizer Module RAM Block Diagram.

2.3.4.4 UART module

For the purpose of data transmission or receiving the necessary information from an external device, we needed a communication module. Thus, we included a serial link (RS-232) module named as *UART Module* to perform this task.

UART module performs an asynchronous communication link as it indicates, *Universal Asynchronous Receiver Transmitter*. Thus, in order to make both sides of the link works "*synchronously*" and transmit or receive the information successfully, we had to define the same communication speed on both sides. In case of communication speed, although, it was possible to design a variable speed UART module, we preferred to use 115200 bit/s static link speed which is the fastest available. In order to match the defined speed, we had to control each individual clock cycle precisely since we don't have a microcontroller with predefined transmission protocols. For instance, when we would like to transmit a HIGH bit at 115200 bit/s communication speed, we had to hold the link at state 1 for 868 clock cycles at 100 MHz clock speed. This value is calculated in terms of desired communication speed and also the clock speed of the system as shown in following equations.

$$T = \frac{1}{115200} \tag{2.2}$$

$$C = \frac{T}{P} \tag{2.3}$$

$$= \frac{T}{10x10^{-9}} \tag{2.4}$$

$$= 868 \tag{2.5}$$

T: Time to transmit a single bit

P: Period of 100 MHz clock frequency (10 ns)

C: Number of clock cycles to transmit a single bit

As a second option for "*synchronization*" of the link, which is also the standard of RS-232 communication protocol, we had to transmit a "*START*" bit and a "*STOP*" bit after transmitting 8 bits of data. In total, it takes 8680 clock cycles (or 86.8 μs) to transmit a frame of data, 10 Bits, in UART link as shown at the bottom of figure 2.15.

Furthermore, in case of transmitting the measurement results which consists of 9 pieces of 24 bit data, we had to define a new protocol. Thus, first we located a header byte to the transmission queue which is 127 in decimal form or equal to "*01111111*" in binary form. Second, we separated the 24 Bit data packages into 8 bit parts to be able to transmit them using our UART link. This process is visualized in figure 2.15.

UART module also receives incoming bytes for system control. Data receiving procedure works in a similar way as transmitting. When the receiver part of the UART module identify the start bit of incoming data, it begins recording each coming bit by counting the individual clock cycles. Finally, it converts the total serial data to parallel form.

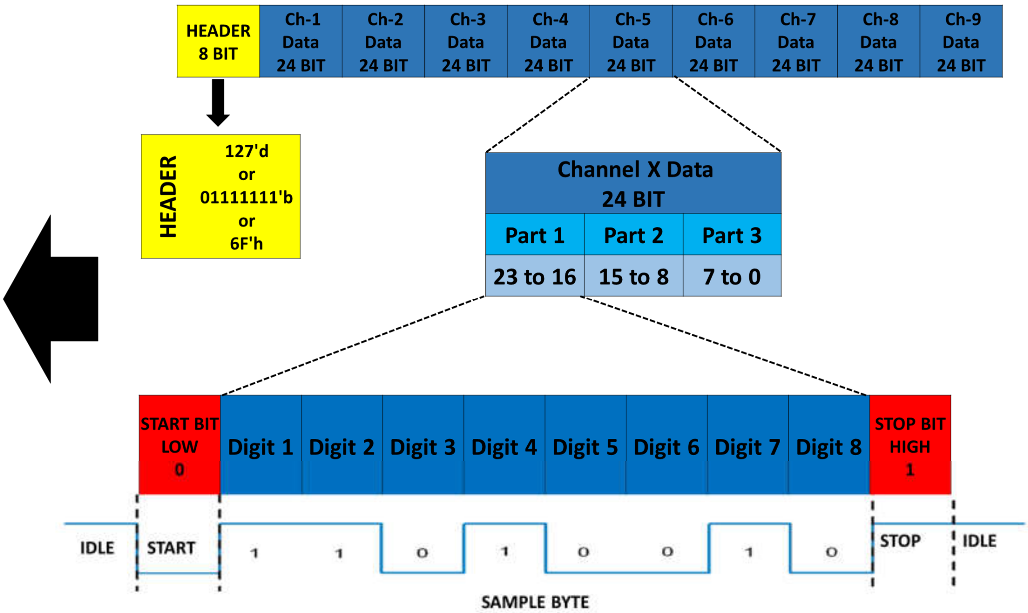

Figure 2.15 : Data frame of FPGA design.

2.3.4.5 Device controller module

Since we designed and developed a complete device, we needed a two way communication link. *UART Module* performs this task; however, for converting the received data to a meaningful information, we designed this dedicated module. UART link always stands in listening mode and when a data, or command is received, it is processed by *Device Controller Module* and converted to meaningful information.

For this system, we defined three main commands: *Start*, *Stop* and *Reset*. For instance, we defined a specific byte, which is hex character "*A*" and equal to "*01000001*" in binary format as *Start* command for starting the measurement process. When the corresponding byte is received, *Device Controller Module* sets a corresponding flag in *Stopwatch Module* and *Pulse Counter Modules* and the counting process is started. This is similar for stop process which is the opposite of start process. We used hex character "*B*" or in binary "*01000010*" for stop process. Reset process also follows a similar procedure. Instead of starting or stopping the operation, a reset signal resets all pulse counters, restarts *Stopwatch Module* operation, deletes all resulted count values in registers of *Data Organizer Module*, stops *UART Module* operations and starts a new count process. This time we used hex character "*C*", in binary "*01000011*", for applying a reset procedure.

2.3.5 Operation procedure

Figure 2.16 shows the flow chart of the operation steps of the counter. The operation starts with *START* command which is sent through the python graphical user interface (*GUI*) to the FPGA. Then, FPGA starts reading each individual channel at 100 MHz speed for a predefined time period.

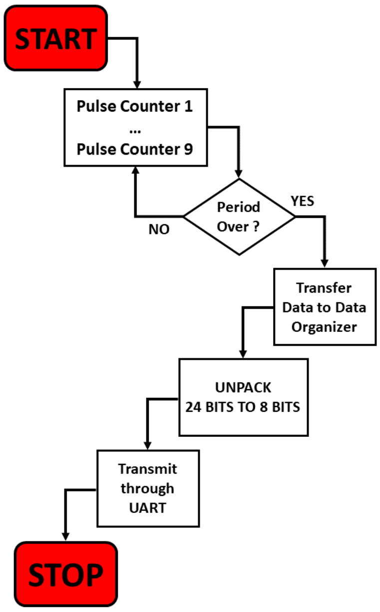

Figure 2.16 : Flow chart of FPGA multi channel counter design.

The end of the measurement period is indicated by *"Period Over"* flag which is set to logic 1 for one clock period, 10 ns. Afterwards, the resulting counts are transferred to *"Data Organizer Module"*. Following the data transfer process, a system reset is applied to each counter for a fresh start. After this moment, two independent processes run at the same time, one is the new counting process and the other one is transmitting the data to Raspberry PI to store and to be able to make further data analysis. At the end, when the data is transmitted, transmission line (TX) goes to *"IDLE"* state and "*Data Organizer Module*" waits for the next *"Period Over"* flag to be set.

The user can reset the FPGA externally with the option available on the GUI. This will stop and restart every individual process in the FPGA hardware. In other words, if transmission process is in progress, it will immediately stop and return to initial *"IDLE"* state and wait for the *"Period Over"* flag to be set again.

2.4 Raspberry PI – Single Board Computer

In this project, a Raspberry PI 3 (*Raspi*) is used for data processing instead of a conventional computer. Raspberry Pi is a credit card sized single board computer developed by the Raspberry Pi Foundation in the United Kingdom (UK) to teach computer science in schools and in developing countries. Very simple connection to the serial link (*TRx*) through GPIO (*General Port for Input and Output*) ports is an advantage of Raspi. There is a direct connection to serial port (*RS232*) which is not available on most new computers. Thus Raspi serves as an ideal data processing environment, providing the results visually, fits into the needs of the detector that we have developed.

Figure 2.17 : Raspberry PI single board computer [19].

2.4.1 Serial link construction

The Raspi equipped with different serial communication links like UART, Bluetooth and Wireless. UART has different options and the one named as miniUART was used here. *UART0 TX* and *UART0 RX* were connected to the header pins 8 and 10. Figure 2.18 shows the Raspberry PI module with its configuration.

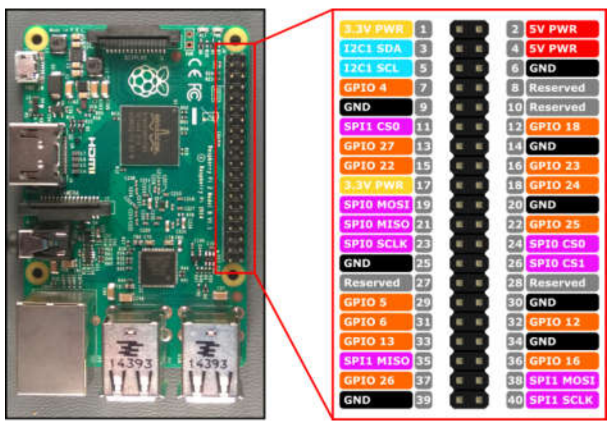

Figure 2.18 : GPIO pin configuration of the Raspberry PI single board computer [20].

2.5 Python Control Interface

Python is an interpreter language with a wide range of applications from web design to hardware control. Thus, we decided to construct the readout software using Python language. We used Python 3.7 version together with some specific packages.

As it is mentioned above and shown in figure 2.15, FPGA transmits the resulting data in three 8-Bit portions. The FPGA can be controlled in command line mode. However, a graphical user interface can simplify the operation. Thus, Python with "*Tkinter*" package was used to build a GUI which is shown in figures 2.19 and 2.20.

As it is presented in figure 2.19, basic functions *"START"*, *"STOP"* and *"RESET"* are located as buttons in the GUI. In addition, since 3x3 matrix detector array is going to be used, results of the instant measurements can be monitored on the first tab of GUI shown in figure 2.19. Also, the total counts can be seen as a graph on the second tab of GUI as shown in figure 2.20.

Additionally, we used *Serial* package for constructing the UART link on Raspi. This gave us an opportunity to transmit the commands and receive the measurement data through the UART link. However, we needed another package to run GUI and UART link together. We used *Threading* package to run two independent processes.

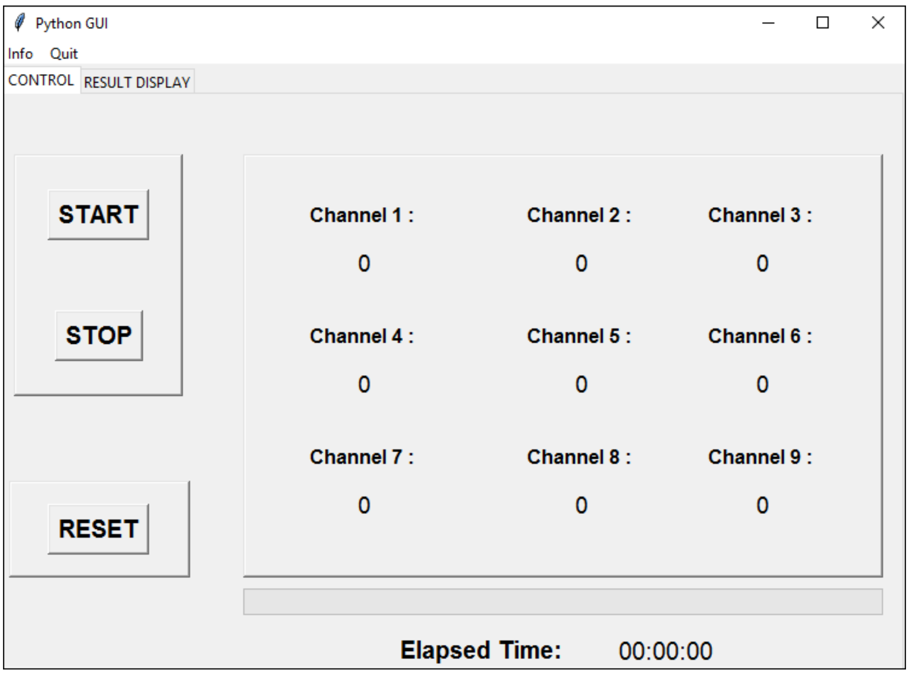

Figure 2.19 : Device control tab of Python graphical user interface for multi channel counter system.

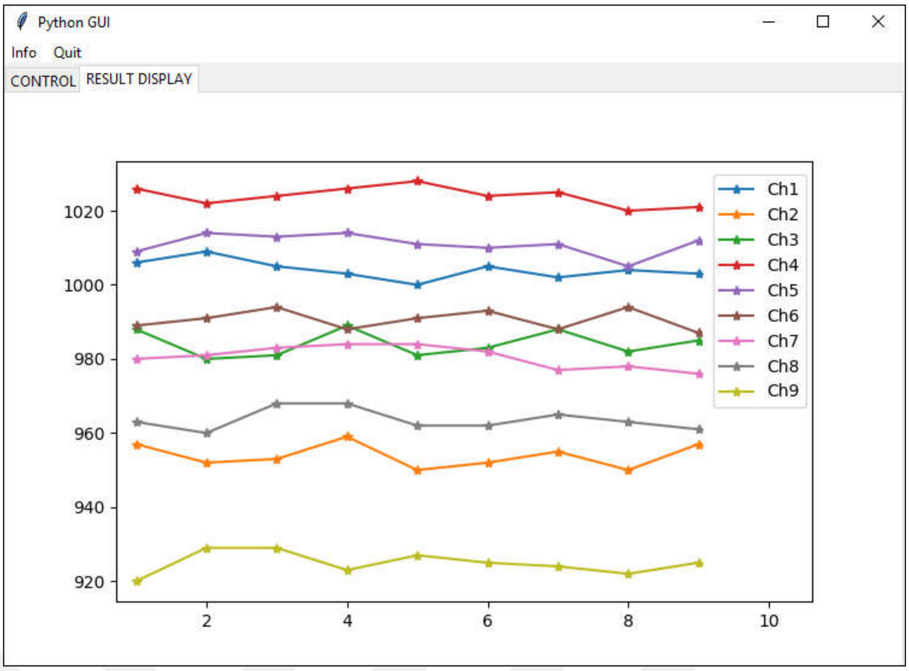

Figure 2.20 : Plot tab of Python graphical user interface for multi channel counter system.

2.5.1 Principle of operation

In case of transmission of *START*, *STOP* and *RESET* commands from the host computer (Raspi) to the FPGA, corresponding bytes defined in FPGA are transmitted through the TX link of the host as described above.

Unlike the Tx line, the operation of Rx line is more complicated due to the system requirements. Receiving data structure is summarized in figure 2.15. The complete data frame is presented at the top which contains a header byte and followed by nine separate 24-Bits long data. Each of these 24-Bits are corresponding to the counting result of the specific channel. However, due to the limits of UART link, it is only possible to transmit or receive one byte at a time. Hence, we have to unpack 24-Bits of data to 8-Bit parts and transmit in three bunches. This operations performed in FPGA and 8-bit long data parts are transmitted this way. When the last byte is transmitted, FPGA completes one loop of the measurement process. Thereafter, once the back-end routine on the host computer identify the header byte coded as 127 (Figure 2.21), it starts counting the received bytes up to 27 corresponding to 27 bytes from nine sensor channel. This is followed by repacking all 8-Bit data parts and composing the counting result on the host computer.

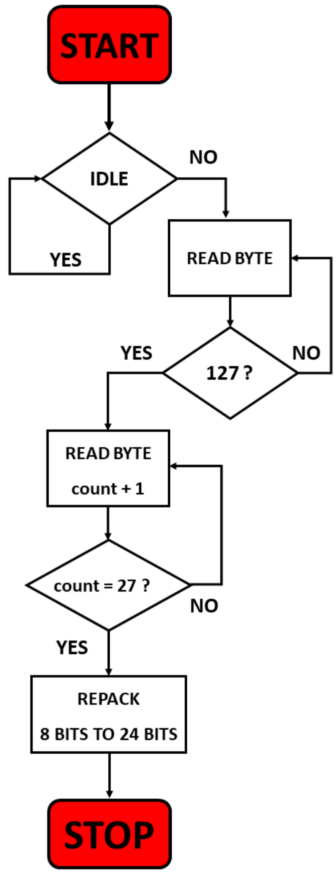

Figure 2.21 : Flow chart of Python readout script for reordering the incoming 8-Bit data packages.

2.6 Complete Device Overview

The final form of the complete detection system is shown in figure 2.22. The detector box is located on the right, the Raspi is in the middle and the python control graphic user interface is also visible on the figure. Additionally, in figure 2.23, the internal structure of the detector box is visible. The sensor module is mounted to the cover from below. The main amplifier module is mounted just below the *Sensor Module*. Heat removal fan is mounted above the main power supply circuit providing $\pm$ 6V.

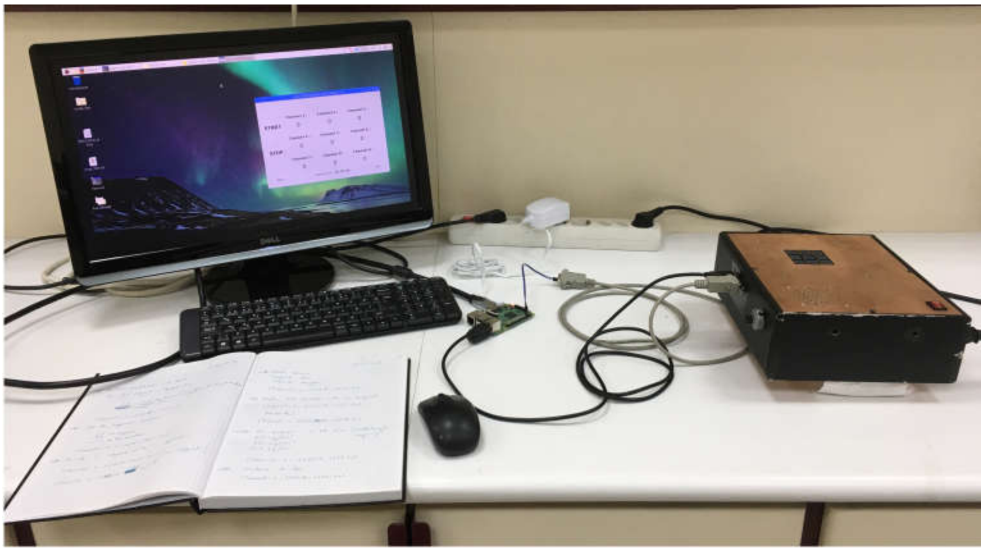

Figure 2.22 : Complete device overview for the desktop measurements.

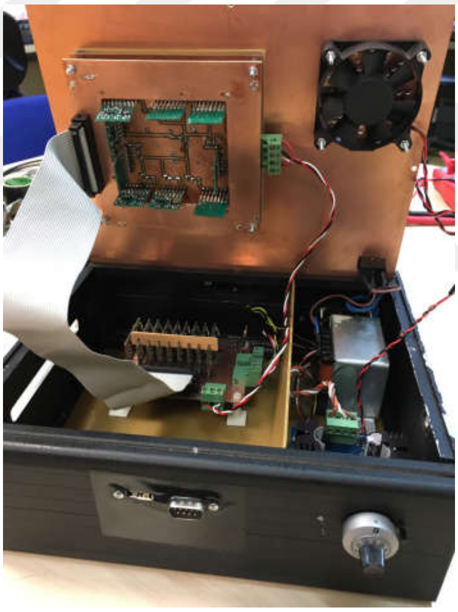

Figure 2.23 : Detector box internal view.

2.7 Spectroscopic Measurements Setup

Although a complete detection system including the necessary signal conditioning electronics and the readout link were designed, performing a spectroscopic measurement will require little more hardware. A Canberra Spectroscopy Amplifier, Model 2020 as shown in figure 2.24 was used for recording the energy spectra. Since the spectroscopy amplifier has only one channel, only one channel out of nine was used.

2.7.1 Canberra spectroscopy amplifier model2020

Canberra spectroscopy amplifier is a NIM module with a relatively simple user interface. It provides variable shaping time and gain settings including coarse and fine tune adjustment. Shaping time constant ranges from 0.25 μs to 6 μs with a "x2" multiplier. These values can be extended up to 12 μs. The coarse gain of the amplifier varies from x10 to x3000 which was fairly enough for all measurements. The *unipolar* and *bipolar* signal outputs are also available for different applications [42].

Figure 2.24 : Canberra spectroscopy amplifier model 2020.

2.7.2 Amptek multichannel analyzer

Spectroscopic measurements have been performed using the Amptek MCA8000A multichannel analyzer (Figure 2.25) [43]. This is a compact and easy-to-use device and it stores the spectra in a text format giving us an opportunity to transfer the spectrum data between the platforms for further data analysis.

Figure 2.25 : Amptek MCA8000A multichannel analyzer.

3. MEASUREMENTS

A series of measurements were performed using various standard radioactive sources to determine the limits of the detector. A crosstalk check between the channels and alpha particle detection efficiency measurements were performed using 5 μCi ^{226}Ra source. ^{241}Am, ^{152}Eu, ^{207}Bi, ^{60}Co and ^{137}Cs standard sources were used to perform the gamma ray measurements. Finally, more measurements were carried out using 3 Ci Am-Be neutron howitzer from J.L. Shepherd and Associates to materialize the actual purpose of the detector, the neutron detection.

The measurements were performed through two different setups. First one was the FPGA controlled counting measurement setup as mentioned before and explained in detail. The second one was for the spectroscopic measurements using a NIM spectroscopy amplifier which was connected to the charge sensitive preamplifier output through a coaxial cable together with an Amptek MCA8000A multi channel analyzer.

3.1 Determination of Cross Talk Using ^{226}Ra Standard Source

Crosstalk is a disturbance, caused by electromagnetic interference, along a circuit or a cable pair. A communication signal disrupts a signal in an adjacent circuit and can cause the signals to become confused and cross over each other. This was possible case for the detector designed since nine signal channels measure the particle radiations independently.

Crosstalk study was performed using 5 μCi ^{226}Ra standard alpha source. It is known that alpha particles have low penetration depth in any medium. They will deposit their energy completely in silicon layer and this will result in production of a large electrical signal. Therefore, to check the crosstalk using an alpha source would be ideal. Relatively large energy deposition of alpha particles results in high count rate, which lead us to determine the cross talk in a shorter measurement period. 30 minutes of total measurement time provides statistically significant cross talk data.

^{226}Ra source is positioned over one of the sensors and leaked counts on the other channels were successively recorded for this measurement. Since the leaked count rate is very small, the numbers are given as the average of all other channels in table 3.1. Calculations have been done using 3.1 and 3.2 as an example for channel 1.

$$C_1 = 1 = \frac{N_1}{N_1} \tag{3.1}$$

$$C_T = \frac{C_2 + C_3 + C_4 + C_5 + C_6 + C_7 + C_8 + C_9}{N_1} \tag{3.2}$$

Although the leaked counts are significantly small, the main reason is the parallel and relatively long ribbon cable used for transferring the signal from the sensor module to the main amplifier module. As it is known, coaxial cables are used for this kind of purposes. However, because of the limited space and required flexibility, we preferred to use a ribbon cable.

Table 3.1 : Crosstalk test results using ^{226}Ra.

Channel No.	C_X	C_T
1	1	16.0x10^{-6}
2	1	4.4x10^{-6}
3	1	6.1x10^{-6}
4	1	35.0x10^{-6}
5	1	18.0x10^{-6}
6	1	66.0x10^{-6}
7	1	21.0x10^{-6}
8	1	17.0x10^{-6}
9	1	18.0x10^{-6}

3.2 Spectroscopic Measurements with ^{226}Ra as an Alpha Source

The kinetic energy of the proton, emitted from the neutron converter materials will be less than 4.601 MeV (5.5%) and 4.784 MeV (94.5%) ^{226}Ra alpha energies. Am-Be neutron source has an average neutron about 4.5 MeV.

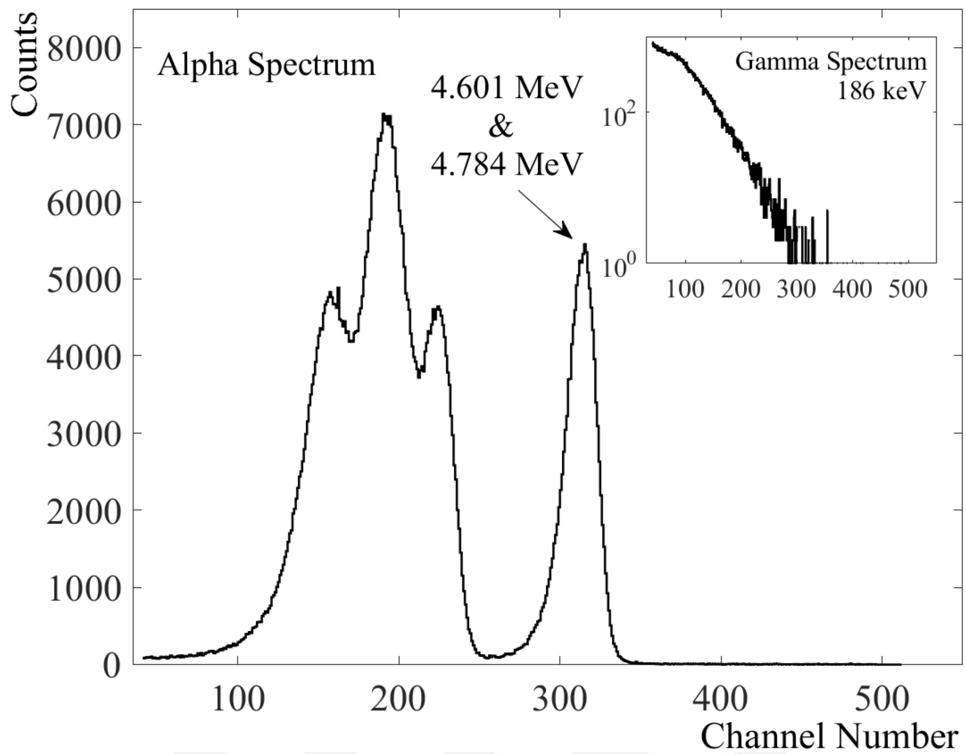

Figure 3.1 : ^{226}Ra alpha and gamma spectra.

A series of measurements were performed to find the optimum amplifier gain to record the spectrum of Am-Be source. In Figure 3.1, Radium spectra with the final settings is shown. Here, the peak on the right is due to the combination of two alpha energies mentioned above. It is not possible to separate two alpha energies because of the poor energy resolution of our new detector.

Furthermore, in the low energy region, a "Mexican Hat" is visible. This triple peak arises from the enclosure shape of ^{226}Ra source which is positioned in a tiny cylindrical barrel (Figure 3.2). The source itself, because of the safety issues, is positioned away from the surface, couple of millimeters inside the barrel. We believe the scattered alpha particles lose some energies which result in the "Mexican Hat" in the spectrum.

Radium has also 186 keV strong gamma line. It is the fact that gamma photons leave little energy in Silicon in contrast to the alpha particles even if they have the same energy. In order to observe 186 keV gamma line of Radium, the amplifier gain was increased 10 times than the one used for alpha measurements. The gamma spectra is shown in the upper right corner of figure 3.1.

Figure 3.2 : Photograph of 5 μCi ^{226}Ra standard radiation source.

3.3 Gamma Measurements

The neutron detection system is designed to be sensitive to the charged particles. However, Am-Be neutron source has also a strong 59.5 keV gamma line originating from the decay regime of natural ^{241}Am. This was an opportunity to study the gamma response of the detector together with the neutrons simultaneously.

Gamma measurements were performed with ^{60}Co, ^{137}Cs, ^{152}Eu, ^{237}Bi and ^{241}Am standard sources. A single detector element was used and sources were positioned directly to the top of the photodiode. Since ^{137}Cs had relatively higher activity, it was positioned 5 cm above the photodiode to reduce the pile-up events.

A combined spectra is shown in Figure 3.3. Here each spectrum was normalized to its maximum value. Also, the energy calibration was performed by determining the endpoints of the ^{241}Am, ^{137}Cs and ^{60}Co spectra. The linearity of the energy calibration can be seen in Figure 3.4.

The ^{241}Am, ^{137}Cs and ^{60}Co sources have strong gamma lines at 59.6 keV, 661.6 keV and 1252.9 keV (as the average of 1173.2 keV and 1332.5 keV of ^{60}Co) respectively. Since 1173.2 keV and 1332.5 keV gamma photons are equally intense and the detection efficiencies of these energies are similar, we used the average energy of the

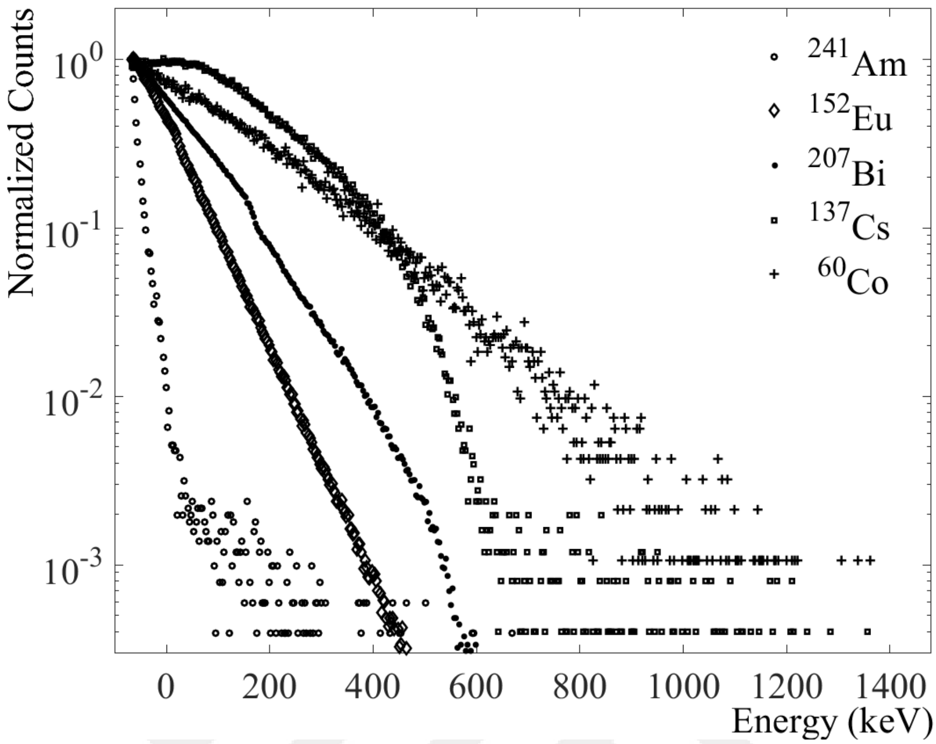

Figure 3.3 : Normalized spectra of ^{241}Am, ^{152}Eu, ^{237}Bi, ^{137}Cs and ^{60}Co gamma sources

two peaks for the calibration. The linear calibration curve given in figure 3.4 proves that this approach is correct. ^{237}Bi has gamma lines at 569.7 keV, 1063.7 keV and 1770 keV and intensities of them are 98%, 75% and 7%, respectively. Since the detection efficiency is relatively larger at low energies, it is expected the endpoint of the spectrum of ^{237}Bi is dominated by 569.7 keV gamma line. This can be seen in figure 3.3. This is valid also for ^{152}Eu but it is not that simple to explain as ^{237}Bi was explained. Unfortunately, ^{152}Eu has many strong gamma lines ranging from 121.8 keV to 1408 keV.

3.4 Gamma Measurements for Am-Be Neutron Source

J.L. Sheppard Am-Be neutron howitzer (Figure 1.1) with 3 Ci ^{241}Am activity has been used as the neutron source. ^{241}Am has a strong gamma line at 59.5 (% 35.9) keV which is highly detectable by a 300 μm Si-PIN photodiode sensor. Figure 3.5 shows the spectra taken at the outer irradiation port of Howitzer type Am-Be source. 59.5 keV gamma contribution to Am-Be spectrum can be seen in the low energy part of the spectrum. Detection efficiency for gamma rays above this energy drops dramatically, therefore gamma rays originated from the excitement of the Carbon atom above 4.4 MeV cannot be detected efficiently in our detector. The spectrum given in Figure 3.5, recorded for 30 minutes, has contributions both from gamma rays and direct neutron interactions with Silicon.

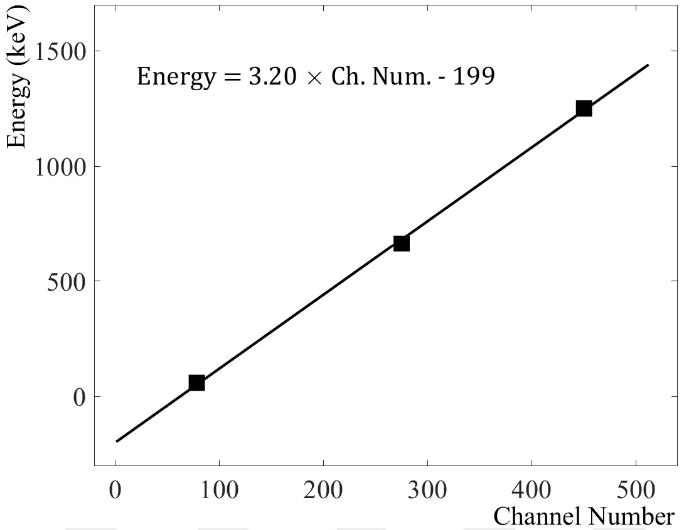

Figure 3.4 : Energy calibration using ^{241}Am, ^{137}Cs and ^{60}Co gamma sources.

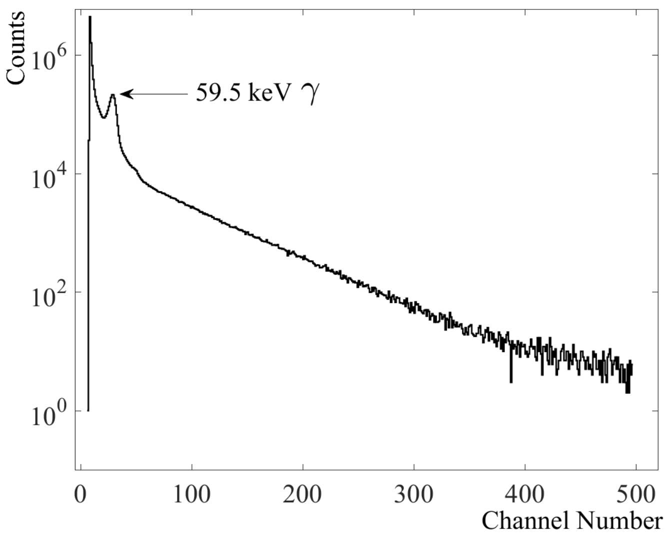

Figure 3.5 : Gamma spectra of Am-Be source for 30 minutes time period.

3.5 Neutron Measurements with Hydrogen Rich Converter Materials

Neutron detection tests have been carried out with and without the converter materials. For building a low-cost detection device, we preferred to use materials easily available like paraffin, high density polyethylene (HDPE), silicone stick glue, Plexiglas and fiberglass cloth with epoxy resin (FR4). These materials were attached in front of the detector array and exposed to neutrons by positioning it perpendicular to the axis of the irradiation port of Am-Be neutron source. Detector-source distance was around 50 cm at this irradiation position.

Data was collected with both measurement setups, the event counting and the spectroscopic. The shaping times were different for both data collection methods and therefore the noise background was slightly higher for the FPGA based detection system. Integral MCA counts above channel 58, corresponding to 280 mV in 5V scale, provided comparable results with the hard thresholded FPGA. Table 3.2 shows the comparison of MCA and FPGA counts with and without the converter materials. These measurements were performed for 30 minutes.

Table 3.2 : Counts compared from the two measurements. The measurement time was set to 30 minutes.

	No Conv.	FR4	Plexiglass	Silicon	HDPE	Paraffin
FPGA	1500	2954	2992	3074	3038	3147
MCA	1412	2863	3034	3096	2960	3157

Figure 3.6 shows the comparison of the naked neutron spectrum and the spectra obtained when various converter materials were used. As seen from the figure, there are visible differences in the detected spectra especially at high energies. Spectral difference above channel 200 is due to the contribution of protons produced from the fast neutrons in the converter materials.

To determine the most sensitive region from the spectral measurements for the separation of fast neutrons, each spectrum in figure 3.6 was integrated between channel i and 1024 (Eq. 3.3) where i is dynamically changed between 30 and 300.

$$F_i = \sum_{j=i}^{1024} c_{ji}, \qquad i = 30 - 300, 30 \tag{3.3}$$

$$N_i = \sum_{j=i}^{1024} n_{ji}, \qquad i = 30 - 300, 30 \tag{3.4}$$

$$D_i = \frac{F_i}{N_i}, \qquad i = 30 - 300, 30 \qquad (3.5)$$

New data sets for each case in figure 3.6 were constructed with incremental steps between 30 and 300 for i. The same procedure performed for the naked spectrum (Eq. 3.4). Data sets for the converter materials were then normalized (Eq. 3.5) to the one obtained from the naked spectrum. Figure 3.7 shows the results from this procedure.

Figure 3.7 shows that the optimum fast neutron separation channel is 200 for all converter materials. However, statistics become limited for channels above 200.

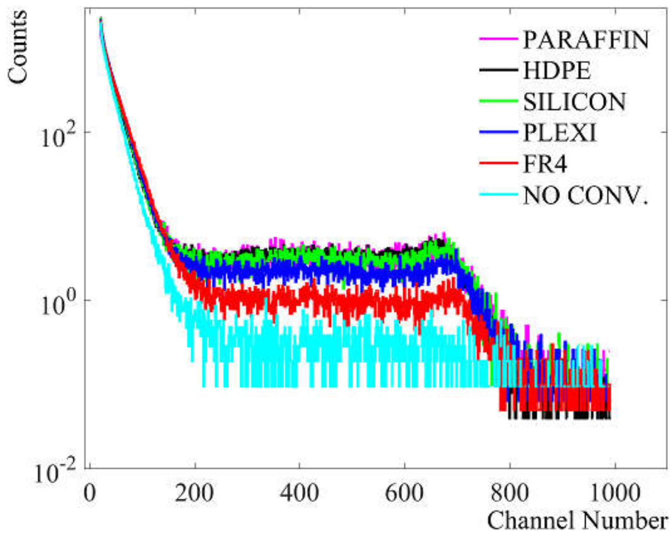

Figure 3.6 : Neutron spectra with different converter materials.

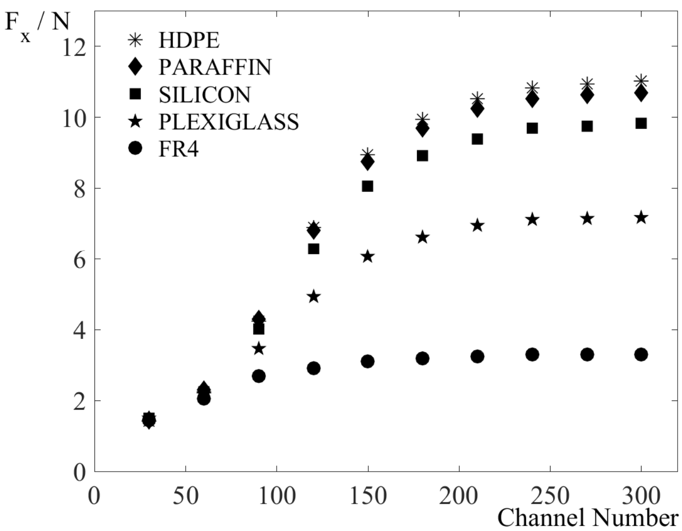

Figure 3.7 : Ratio of the integral counts above LLD with converters to the counts recorded without any converter.

4. CONCLUSION

Through over a period of about four years, this thesis work consists of two basic stages. In the first stage, a single silicon PIN photodiode and different neutron proton converter materials were used for early tests of the radiation detection. After obtaining the successful results, the existing nine channel version was designed and produced. The measurements showed that the additional eight sensors made detection efficiency increase by 9-fold as expected. However, the cost was the complexity of simultaneous readout of 9 channels.

Test measurements have been carried out for different types of radiation in addition to neutrons. In case of a possible crosstalk between different sensor channels, a ^{226}Ra alpha source was used. Tests with ^{226}Ra alpha source showed that none of the channels had significant cross talk. This result shows that the number of sensors or channels can be safely increased. The Am-Be neutron source used for neutron measurements is known to be a mixed neutron gamma radiation source. Thus, spectroscopic measurements were made by connecting an external NIM spectroscopy amplifier, running faster than the current system, to one of the preamplifiers feeded by silicon PIN photodiodes. The aim of this method was to obtain detailed information about the conversion efficiency of different neutron proton converter materials. The subsequent counting measurements gave consistent results with the spectroscopic measurements. Since the Am-Be source, used in the neutron measurements, has also a natural gamma line, independent measurements have been carried out to obtain low energy gamma detection capability of the detector. ^{241}Am, ^{152}Eu, ^{207}Bi, ^{60}Co and ^{137}Cs sources were also used to figure out the gamma response up to 1408 keV. Gamma rays are expected to produce a signal at a lower amplitude than neutron-derived proton and this was observed as well. Thus, the NIM spectroscopy amplifier system, which adjusts the signal amplification rate 10 times higher than that used for the neutron measurements, has shown that gamma detection can be performed with the current system at low efficiency. In addition, the ten-fold increase in the amplification gain made it clear that there is no significant contribution from gamma rays to the neutron spectra.

This detector is considered to be the most critical part of a buried explosive detection system based on neutron scattering. As a result, a detector system for the detection of fast neutrons has been designed and successfully tested. The success achieved in the test results can be considered as the first step for a more accurate and efficient system in the future. Accordingly, a new detector design can be made using a larger number of silicon PIN photodiodes to cover larger detection area. In case of different neutron energies, especially for thermal region, ^{10}B and ^{6}LiF will be the excellent choices based on the studies in the literature. A much better study would be to made is to combine different neutron converter materials (and possibly thicknesses) to detect the neutrons with wider energy range. This can be achieved by making an array of individual silicon PIN photodiodes which are coated with ^{10}B, ^{6}LiF and hydrogen rich materials (PE, paraffin etc.).

REFERENCES

[1] **Hoste, J.** (1988). Isotopic neutron sources for neutron activation analysis user's manual (IAEA-TECDOC-465)., *International Atomic Energy Agency*.

[2] **Wattenberg, A.** (1949). Photo-Neutron sources, *National Research Council, Division of Mathematical and Physical Sciences*.

[3] **Url-1**, https://www.thermofisher.com/order/catalog/product/1517021A?SID=srch-srp-1517021A, accessed at: 30.04.2019.

[4] **Url-2**, https://www.equipcoservices.com/images/tutorials/introrad2.png, accessed at: 30.04.2019.

[5] **Url-3**, https://www.advatech-uk.co.uk/scintillators_plastic.html, accessed at: 30.04.2019.

[6] **Url-4**, https://www.equipcoservices.com/images/tutorials/introrad1.png, accessed at: 30.04.2019.

[7] **Url-5**, https://www.halbleiter.org/en/fundamentals/conductors-insulators-semiconductors/, accessed at: 30.04.2019.

[8] **Url-6**, https://www.electronics-notes.com/images/diode-photo-pin-structure-01.svg, accessed at: 30.04.2019.

[9] **Url-7**, https://www.aptechnologies.co.uk/images/img/ODC/PV_and_PC_Modes.png, accessed at: 30.04.2019.

[10] **Yang, H.**, **Menaa, N.**, **Bronson, F.**, **Kastner, M.**, **Venkataraman, R. and Mueller, W.** (2011). Evaluation of a LiI(Eu) neutron detector with coincident double photodiode readout, *Nuclear Instruments and Methods in Physics Research Section A: Accelerators, Spectrometers, Detectors and Associated Equipment*, *652*(1), 364–369.

[11] **Fioretto, E.**, **Innocenti, F.**, **Viesti, G.**, **Cinausero, M.**, **Zuin, L.**, **Fabris, D.**, **Lunardon, M.**, **Nebbia, G. and Prete, G.** (2000). CsI(Tl)-photodiode detectors for gamma-ray spectroscopy, *IEEE Transactions on nuclear science*, *47*(4), 1315–1318.

[12] **Voytchev, M.**, **Iniguez, M.**, **Mendez, R.**, **Mananes, A.**, **Rodriguez, L. and Barquero, R.** (2003). Neutron detection with a silicon PIN photodiode and 6LiF converter, *Nuclear Instruments and Methods in Physics Research Section A: Accelerators, Spectrometers, Detectors and Associated Equipment*, *512*(3), 546–552.

[13] **Adamiec, G., Iñiguez, M., Lorente, A., Voytchev, M. and Gallego, E.** (2004). Response of a silicon PIN photodiode to an Am-Be neutron source, *Nuclear Instruments and Methods in Physics Research Section A: Accelerators, Spectrometers, Detectors and Associated Equipment*, *534*(3), 544–550.

[14] **Mesquita, C., Filho, T. and Hamada, M.** (2003). Development of neutron detector using the PIN photodiode with polyethylene (n, p) converter., *IEEE Transactions on Nuclear Science*, *50*(4), 1170–1174.

[15] **Url-8**, `https://www.cadsofteagle.de`, accessed at: 30.04.2019.

[16] First Sensor Corporation, (2012). Datasheet.

[17] **Url-9**, `https://www.xilinx.com/html_docs/xilinx2017_2/sda/ccel_doc/topics/images/basic_fpga.png`, accessed at: 30.04.2019.

[18] **Url-10**, `https://www.aessent.com/`, accessed at: 30.04.2019.

[19] **Url-11**, `https://www.raspberrypi.org`, accessed at: 30.04.2019.

[20] **Url-12**, `https://www.raspberrypi.org/documentation/usage/gpio/`, accessed at: 30.04.2019.

[21] **Krane, K.**, (1987). Introductory Nuclear Physics, John Wiley and Sons, Inc., Oregon, 1. edition.

[22] **Reuse, P.**, (2008). Neutron Physics, EDP Sciences, USA, 1. edition.

[23] **Knauer, J. and Martin, R.**, (1997). Californium-252 production and neutron source fabrication, Springer, pp.7–24.

[24] **Chichester, D.L.**, (2012). Production and applications of neutrons using particle accelerators, World Scientific, pp.243–305.

[25] **Almenas, K. and Lee, R.**, (1992). Nuclear Engineering: An Introduction, Springer, Berlin, pp.53–82.

[26] **Knoll, G.F.**, (1999). Radiation detection and measurement, John Wiley & Sons, Ann Arbor, Michigan, pp.53–57.

[27] **Cerrito, L.**, (2017). Radiation and Detectors: Introduction to the Physics of Radiation and Detection Devices, Springer, London, 1. edition.

[28] **Wang, W.C.**, (2011). Optical Detectors, National Tsing Hua University., Beijing, 1. edition.

[29] **Ryzhikov, V., Danshin, E., Lubimskii, W., Smirnov, N., Zelenskaya, O., Filimonov, A. and Chernikov, V.** (1997). Measurements of fluxes of thermal neutrons using detector ^{6}LiI(Eu)-Si-Pin-Pd and a charge-sensitive preamplifier, *Nuclear Science Symposium*, IEEE, Albuquerque, NM, USA, pp.767,768.

[30] **Totsuka, D.**, **Yanagida, T.**, **Fukuda, K.**, **Kawaguchi, N.**, **Fujimoto, Y.**, **Pejchal, J.**, **Yokota, Y. and Yoshikawa, A.** (2011). Performance test of Si PIN photodiode line scanner for thermal neutron detection, *Nuclear Instruments and Methods in Physics Research Section A: Accelerators, Spectrometers, Detectors and Associated Equipment*, *659*(1), 399–402.

[31] **Kawaguchi, N.**, **Yanagida, T.**, **Fujimoto, Y.**, **Furuya, Y.**, **Futami, Y.**, **Yamaji, A.**, **Watanabe, K.**, **Yamazaki, A.**, **Uritani, A.**, **Kajimoto, S.** *et al.* (2013). Neutron detection with LiCaAlF6 scintillator doped with 3d-transition metal ions, *Radiation Measurements*, *55*, 128–131.

[32] **McGregor, D.S.**, **Klann, R.T.**, **Sanders, J.D.**, **Lindsay, J.T.**, **Linden, K.J.**, **Gersch, H.K.**, **De Lurgio, P.**, **Fink, C.L. and Ariesanti, E.** (2003). Recent results from thin-film-coated semiconductor neutron detectors, *X-Ray and Gamma-Ray Detectors and Applications IV*, volume4784, International Society for Optics and Photonics, Seattle, WA, USA, pp.164–183.

[33] **Cárdenas, J.P.N.**, **Campos, L.L. and Filho, T.M.** (2011). Evaluation of a PIN Photodiode Detector in Neutron-Gamma Fields, *AIP Conference Proceedings*, volume1351, AIP, pp.242–247.

[34] **Guardiola, C.**, **Fleta, C.**, **Quirion, D.**, **Rodríguez, J.**, **Lozano, M.**, **Teixidor, F.**, **Viñas, C.**, **Popescu, A.**, **Domingo, C. and Amgarou, K.** (2011). First investigations of a silicon neutron detector with a carborane converter, *Journal of Instrumentation*, *6*(11), P11001.

[35] **Kang, K.**, **Jeon, H.**, **Kim, G.**, **Park, H.**, **Hyun, H. and Kah, D.** (2014). Response of a photodiode coupled with boron for neutron detection, *Journal of the Korean Physical Society*, *65*(9), 1374–1378.

[36] **Hosono, Y.**, **Iguchi, T.**, **Nakazawa, M.** *et al.* (1995). Fast neutron detector using PIN-type silicon photodiode, *Nuclear Instruments and Methods in Physics Research Section A: Accelerators, Spectrometers, Detectors and Associated Equipment*, *361*(3), 554–557.

[37] **Fei, J.**, **Huang, Y.**, **Liu, T.**, **Ma, X.**, **Duan, X.**, **Liu, K. and Ren, X.** (2017). Performance comparison between serial-connected and parallel-connected photodiode array, *Lasers and Electro-Optics (CLEO), 2017 Conference on*, IEEE, pp.1–2.

[38] **Bayrak, A.** (2012). Design and optimization of radon field monitor based on silicon PIN photodiodes, *Ph.D. thesis*, İstanbul Technical University, İstanbul, TURKEY.

[39] **Emirhan, E.**, **Bayrak, A.**, **Yücel, E.B.**, **Yücel, M. and Ozben, C.** (2016). A low cost X-ray imaging device based on BPW-34 Si-PIN photodiode, *Nuclear Instruments and Methods in Physics Research Section A: Accelerators, Spectrometers, Detectors and Associated Equipment*, *819*, 1–5.

[40] Maxim Intgerated Company, (2019). Datasheet.

[41] **Url-13**, https://www.xilinx.com/products/design-tools/ise-/design-suite.html, accessed at: 30.04.2019.

[42] **Url-14**, https://www.mirion.com/products/2020-spectroscopy/-amplifier, accessed at: 30.04.2019.

[43] **Url-15**, http://amptek.com/products/, accessed at: 30.04.2019.

CURRICULUM VITAE

Name Surname: Ahmet BAYRAK

Place and Date of Birth: Gerze - 23.01.1985

E-Mail: bayrakah@itu.edu.tr

EDUCATION:

- **B.Sc.:** 2009, ITU, Faculty of Science and Letters, Physics Engineering Department
- **M.Sc.:** 2012, ITU, Graduate School of Science, Engineering and Technology

PROFESSIONAL EXPERIENCE AND REWARDS:

- 2018- : TUBITAK Marmara Research Center (MAM), Senior Researcher
- 2010-2018 : ITU Physics Engineering Department, Research Assistant
- 2012-2013 : Brookhaven National Laboratory (BNL), Visiting Researcher (2 months)
- 2016-2017 : Deutsches-Elektronen Synchrotron (DESY), Visiting Researcher (1 year)

PUBLICATIONS, PRESENTATIONS AND PATENTS ON THE THESIS:

- **Bayrak, A.**, Yucel, M., Yucel, E.B., Ozben, C.S., 2019. A Segmented Neutron Detector Based on Si-PIN Photodiodes and Neutron-Proton Converters. *Nuclear Technology and Radiation Protection Journal,* Vol. 34, No. 2.
- **Bayrak, A.**, Yucel, M., Yucel, E.B., Ozben, C.S., 2018. Design and Development of an FPGA Controlled Silicon PIN Photodiode Detector Array for Neutron Detection. *Ankara University, Institute of Nuclear Sciences, Graduate Student Congress*, May 11-13, 2018, Ankara, Turkey. (oral presentation)
- Yucel, M., **Bayrak, A.**, Yucel, E.B., Ozben, C.S., 2018. Simulations of Si-PIN Photodiode Based Detectors for Underground Explosives Enhanced by Ammonium Nitrate, *Nuc. Ins. & Met. In Phy. Res. Sec. A-Acc. Spect. Det. And Associated Eq.,* Vol. 880, 152-157.
- Emirhan, E., **Bayrak, A.**, Yucel, E.B., Yucel, M., Ozben, C.S., 2016. A low cost X-ray imaging device based on BPW-34 Si-PIN photodiode, *Nuc. Ins. & Met. In Phy. Res. Sec. A-Acc. Spect. Det. And Associated Eq.,* Vol. 819, 1-5
- Yucel, M., Emirhan, E., **Bayrak, A.**, Ozben, C.S., Yucel, E.B., 2015. Comparison of Simulated and Measured Spectra from an X-Ray Tube for the Energies Between 20 and 35 keV, *Nuc. Ins. & Met. In Phy. Res. Sec. A-Acc. Spect. Det. And Associated Eq.,* Vol. 799, 50-53

OTHER PUBLICATIONS, PRESENTATIONS AND PATENTS:

- **Bayrak, A.**, Barlas, E., Emirhan, E., C. Kutlu, Ozben, C.S., 2013. A complete low cost radon detection system, *Applied Radiation and Isotopes,* Vol. 78, 1-9
- Barlas, E., **Bayrak, A.**, Emirhan, E., Haciomeroglu, S., Ozben, C.S., 2013. Spatial Distribution of Po-214 Ions in the Electrostatic Collection, *Applied Radiation and Isotopes,* Vol. 80, 23-26
- Ozben, C.S., **Bayrak, A.**, Emirhan, M.E., Barlas, E., C. Kutlu, 2013. Radon Saha Monitörü (Radon Field Monitor). Patent numarası: 2013/01007
- Ozben, C.S., **Bayrak, A.**, Emirhan, M.E., Barlas, E., C. Kutlu, 2012. 2012. Design and Optimization of Radon Field Monitor Based on Silicon PIN Photodiode. *Workshop on High Energy Physics and Applications*, June 19-23, 2012, Izmir, Turkey. (Presentation)